

Unimodality-Constrained Matrix Factorization for Non-Parametric Source Localization

Junting Chen and Urbashi Mitra

Ming Hsieh Department of Electrical Engineering, University of Southern California
Los Angeles, CA 90089 USA, email: {juntingc, ubli}@usc.edu

Abstract—Herein, the problem of simultaneous localization of multiple sources given a number of energy samples at different locations is examined. The strategies do not require knowledge of the signal propagation models, nor do they exploit the spatial signatures of the source. A non-parametric source localization framework based on a matrix observation model is developed. It is shown that the source location can be estimated by localizing the peaks of a pair of location signature vectors extracted from the incomplete energy observation matrix. A robust peak localization algorithm is developed and shown to decrease the source localization mean squared error (MSE) faster than $\mathcal{O}(1/M^{1.5})$ with M samples, when there is no measurement noise. To extract the source signature vectors from a matrix with mixed energy from multiple sources, a unimodality-constrained matrix factorization (UMF) problem is formulated, and two rotation techniques are developed to solve the UMF efficiently. Our numerical experiments demonstrate that the proposed scheme achieves similar performance as the kernel regression baseline using only $1/5$ energy measurement samples in detecting a single source, and the performance gain is more significant in the cases of detecting multiple sources.

Index Terms—Source localization, unimodal, sparse signal processing, matrix completion, non-parametric estimation

I. INTRODUCTION

Source localization is important in many domains, such as salvage, exploration, tactical surveillance, and hazard finding. However, in many application scenarios, it is difficult to obtain the correct propagation parameters of the source signal for localization. For example, in underwater localization with acoustic signals, the signal propagation depends on the water temperature, pressure, and salinity, which are location-dependent. In gas source localization, the gas diffusion characteristics depends on the chemical type and the atmospheric conditions. Therefore, model-based parametric localization methods [1]–[4] may not be reliable in application scenarios with a temporal and spatial varying nature.

Model-free positioning schemes, such as connectivity based localizations and weighted centroid localizations (WCL), have attracted a lot of interest due to their simplicity in implementation and the robustness to variations of propagation properties [5]–[9]. However, connectivity based techniques [5], [6] can only provide coarse localization results and the performance of WCL [7] highly depends on the choice of parameters and the propagation environments. Recently, machine learning techniques, such as kernel regression and support vector machines

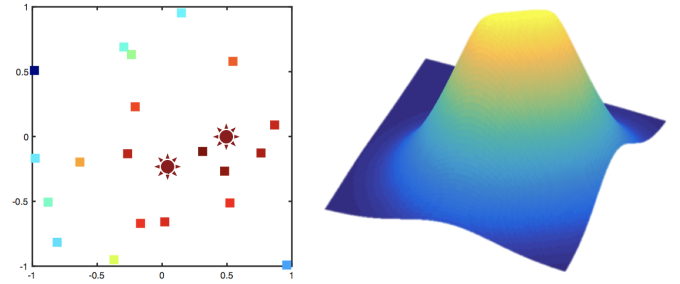


Figure 1. Left: Energy measurements at different locations (colored-squares) to localize two sources (red stars). Right: The underlying energy field appears as one peak when the two sources are close to each other.

[10], [11] have also been explored for localization. However, these methods usually require a separate training phase which may not be available in practice. Furthermore, blind deconvolution methods for source separation and localization [12]–[17] usually require a sequence of measurements that convey temporal or spatial characteristics, which is not the case in our problem.

This paper studies non-parametric methods for localizing several sources based on a few energy measurements at different sensing locations as illustrated in Fig. 1. Our previous works studied the single source case in [8], [18], where a trust region was developed for targeting the source and a multi-step exploration-exploitation strategy was developed for active search using an underwater robot. The results were extended to the cases of two or more sources by exploiting novel coordinate system rotation techniques [9], [19]. However, these works were based on a decomposable assumption on the energy propagation field in 2D.

In this paper, we find that the decomposable assumption is *not* necessary. Specifically, we show that the source location in 2D can be found by localizing the peaks of the left and right dominant singular vectors of the energy matrix sampled on a discretized area. Such a result holds *universally* as long as the received signal energy is a decreasing function of the distance from the source. With such a theoretical guarantee, we first develop strategies to localize a single source. The method extracts a pair of signature vectors from a sparsely sampled observation matrix, and then, estimates the source location by robust peak localization from the signature vectors. The corresponding localization mean squared error (MSE) is also analyzed. We then move to the case of localizing two sources

This research has been funded in part by one or more of the following grants: ONR N00014-15-1-2550, NSF CNS-1213128, NSF CCF-1718560, NSF CCF-1410009, NSF CPS-1446901, and AFOSR FA9550-12-1-0215.

with equal power. The singular value decomposition (SVD) framework in our preliminary work [18] does not work herein, because the singular vectors are not the desired signature vectors of each source. We address this issue by optimally rotating the coordinate system such that the sources are aligned with the rows or columns of the observation matrix, and as a result, the SVD-based method can be applied. Finally, we consider the general multi-source case by formulating a unimodality-constrained matrix factorization (UMF) problem and solve it with projected gradient algorithms. While a formal theoretical justification that connects the multi-source localization with the UMF is yet to be explored, our experiments demonstrate the robustness of the proposed UMF-based methods.

To summarize, the following contributions are made herein:

- We propose a matrix observation model for the energy field of a single source, and prove that the left and right dominant singular vectors are unimodal with their peaks representing the source location.
- We develop non-parametric localization algorithms based on sparse matrix processing. In the single source case, we derive a localization MSE bound and show that the MSE decreases faster than $\mathcal{O}(1/M^{1.5})$ when there is no sampling noise.
- For a general multi-source case, we formulate a UMF problem and develop a projected gradient algorithm to extract the signature vectors for localizing each of the sources. Our numerical experiments demonstrate the robustness of these methods in uncertain environments.

The rest of the paper is organized as follows. Section II establishes the matrix observation model. Section III develops a non-parametric localization estimator by establishing the unimodal and symmetry property of the source signature vectors. Section IV extracts the signature vectors for the single source scenario and analyzes the MSE localization performance. Section V and VI develop coordinate system rotation techniques to help extract the signature vectors in the two source and arbitrary number of sources cases. Numerical results are presented in Section VII and conclusion is given in Section VIII.

Notation: Vectors are written as bold italic letters \mathbf{x} and matrices as bold capital italic letters \mathbf{X} . Random variables, random vectors, and random matrices are written as x , bold letters \mathbf{x} , and bold capital letters \mathbf{X} , respectively. For a matrix \mathbf{X} , X_{ij} denotes the entry in the i th row and j th column of \mathbf{X} . For a vector \mathbf{x} , x_i denotes the i th entry of \mathbf{x} . The notation $o(x)$ means $\lim_{x \rightarrow 0} o(x)/x \rightarrow 0$, and $\mathcal{O}(x)$ means $\limsup_{x \rightarrow 0} \mathcal{O}(x)/x < \infty$.

II. SYSTEM MODEL

Assume that there are K incoherent sources in an area with radius $L/4$. The location of source k is denoted by $\mathbf{s}_k \in \mathbb{R}^2$. The sources continuously emit signals that form an aggregated energy field, which can be measured at M different sensing locations in the target area \mathcal{A} with radius $L/2$. Let $d(\mathbf{z}, \mathbf{s}) = \|\mathbf{z} - \mathbf{s}\|_2$ be the distance between the sensing location at $\mathbf{z} \in$

\mathbb{R}^2 and a source location \mathbf{s} . The energy measurement $h^{(m)}$ at the m th sensing location $\mathbf{z}^{(m)}$ is given by

$$h^{(m)} = \sum_{k=1}^K \alpha_k h(d(\mathbf{z}^{(m)}, \mathbf{s}_k)) + n^{(m)} \quad (1)$$

where α_k is the transmit power of source k and $n^{(m)}$ is the additive noise of the m th measurement. The measurement noise $n^{(m)}$ is modeled as a zero mean random variable with variance σ_n^2 and bounded support $|n^{(m)}| < \bar{\sigma}_n$. The function $h(d)$ is a non-negative strictly decreasing function of the distance d from the source. In addition, we assume that $h(d)$ is Lipschitz continuous, square-integrable, and concentrated in the bounded area \mathcal{A} , i.e., $\int_{\mathbb{R}^2} h(d(\mathbf{z}, \mathbf{s}))^2 d\mathbf{z} = \int_{\mathcal{A}} h(d(\mathbf{z}, \mathbf{s}))^2 d\mathbf{z} = 1$. Note that, in reality, the effective energy response $h(d)$ measured by practical devices always has a bounded support. However, neither the source power α_k , the function $h(d)$, nor the noise distribution are known.

We propose to use a matrix observation model for non-parametric source localization. Specifically, we discretize the $L \times L$ target area, \mathcal{A} , into $N \times N$ grid points, equally spaced with minimum distance $\frac{L}{N}$, $N \geq \sqrt{M}$. Let \mathbf{H} be the $N \times N$ observation matrix that contains the M energy measurements, i.e., the (i, j) th entry of \mathbf{H} is given by

$$H_{ij} = \frac{L}{N} h^{(m)} \quad (2)$$

if the m th energy measurement is taken inside the (i, j) th grid cell. Note that \mathbf{H} may contain missing values and the measurement locations $\mathbf{z}^{(m)}$ may not be at the center of the grid cell. Our objective herein is to localize the sources by analyzing the incomplete matrix \mathbf{H} .

III. LOCALIZATION BASED ON UNIMODALITY

In this section, we first show that the dominant singular vectors of the energy matrix sampled in a discretized single source energy field are unimodal and symmetric. Then, using these properties, a localization algorithm is developed. Finally, a matrix factorization problem is formulated to extract the signature vectors in the case of multiple sources and incomplete matrix observations.

A. The Unimodal Property

Let $\mathbf{H}^{(k)} \in \mathbb{R}^{N \times N}$ be the matrix that captures the energy contributed by source k sampled at discretized locations $\{\mathbf{c}_{i,j}\}$, i.e., the (i, j) th element of $\mathbf{H}^{(k)}$ is given by

$$H_{ij}^{(k)} = \frac{L}{N} \alpha_k h(d(\mathbf{c}_{i,j}, \mathbf{s}_k)) \quad (3)$$

in which, $\mathbf{c}_{i,j} \in \mathbb{R}^2$ is the center location of the (i, j) th grid cell. The factor $\frac{L}{N}$ is for normalization purposes:

$$\begin{aligned} \|\mathbf{H}^{(k)}\|_F^2 &= \alpha_k^2 \sum_{i,j} \left(\frac{L}{N}\right)^2 h(d(\mathbf{c}_{i,j}, \mathbf{s}_k))^2 \\ &= \alpha_k^2 \int_{\mathcal{A}} h(d(\mathbf{z}, \mathbf{s}_k))^2 d\mathbf{z} + o\left(\frac{L^2}{N^2}\right) \end{aligned} \quad (4)$$

which equals to α_k^2 up to a marginal discretization error. In the signal model (3) and (4), the physical meaning of $h(d(x, y))$ is the power density of the source signal measured at location (x, y) and the entry $H_{ij}^{(k)}$ approximates the energy of the k th source signal in the (i, j) th grid cell.

Consider the SVD of $\mathbf{H}^{(k)} = \sum_i \sigma_{k,i} \mathbf{u}_{k,i} \mathbf{v}_{k,i}^T$, where $\sigma_{k,i}$ denote the i th largest singular value of $\mathbf{H}^{(k)}$. Then, we have the following model for the K source energy field.

Definition 1 (Signature vector and signature matrix). The signature matrix for all K sources is defined as

$$\mathbf{H} \triangleq \sum_{k=1}^K \mathbf{H}^{(k)} = \sum_{k=1}^K \sigma_{k,1} \mathbf{u}_{k,1} \mathbf{v}_{k,1}^T + \sum_{k=1}^K \sum_{i=2}^N \sigma_{k,i} \mathbf{u}_{k,i} \mathbf{v}_{k,i}^T. \quad (5)$$

In addition, the vectors $\mathbf{u}_k \triangleq \mathbf{u}_{k,1}$ and $\mathbf{v}_k \triangleq \mathbf{v}_{k,1}$, are defined as the signature vectors of source k .

Note that \mathbf{u}_k and \mathbf{v}_k are not singular vectors of \mathbf{H} , but they are the dominant singular vectors of $\mathbf{H}^{(k)}$, which captures the energy contribution from the k th source.

Accordingly, the observation matrix \mathbf{H} in (2) is a noisy and incomplete sampled version of the signature matrix \mathbf{H} .

We show that the signature vectors \mathbf{u}_k and \mathbf{v}_k are unimodal.

Definition 2 (Unimodal). A vector $\mathbf{v} \in \mathbb{R}^N$ is unimodal if the following is satisfied:

$$0 \leq v_1 \leq v_2 \leq \dots \leq v_s \quad (6)$$

$$v_s \geq v_{s+1} \geq \dots \geq v_N \geq 0 \quad (7)$$

for some integer $1 \leq s \leq N$, where v_i is the i th entry of \mathbf{v} .

Note that there could be multiple entries $v_s = v_{s+1} = \dots = v_{s+I}$ that are the largest. In other words, the vector has a flat peak. This will not affect the algorithm design, nor the analytical results in this paper.

Theorem 1 (Unimodal Signature Vector). *The signature vectors \mathbf{u}_k and \mathbf{v}_k are unimodal. In addition, suppose that source k is located inside the (m, n) th grid cell. Then the peaks of \mathbf{u}_k and \mathbf{v}_k are located at the m th entry of \mathbf{u}_k and the n th entry of \mathbf{v}_k , respectively.*

Proof. See Appendix A. \square

Note that such a property holds for general propagation functions $h(d)$.

B. The Symmetry Property

It can be further shown that the signature vectors \mathbf{u}_k and \mathbf{v}_k are symmetric.

Let \mathbf{u}_k^N and \mathbf{v}_k^N denote the signature vectors under the $N \times N$ grid topology. Consider a Cartesian coordinate system \mathcal{C} and denote $\mathbf{c}_{i,j} = (c_{i,j,1}, c_{i,j,2}) \in \mathbb{R}^2$ as the coordinates of the (i, j) th grid point, where every row of grid points $\{\mathbf{c}_{i,1}, \mathbf{c}_{i,2}, \dots, \mathbf{c}_{i,N}\}$ has the same set of x -coordinates $\mathbf{c}_X = [c_{X,1}, c_{X,2}, \dots, c_{X,N}]$, and every column of grids $\{\mathbf{c}_{1,j}, \mathbf{c}_{2,j}, \dots, \mathbf{c}_{N,j}\}$ has the same set of y -coordinates $\mathbf{c}_Y = [c_{Y,1}, c_{Y,2}, \dots, c_{Y,N}]$. Let $\bar{u}_k^N(y)$ and $\bar{v}_k^N(x)$ be linearly interpolated functions from vectors \mathbf{u}_k^N and \mathbf{v}_k^N , respectively.

Specifically, $\bar{u}_k^N(c_{X,i}) = \sqrt{N/L} u_{k,i}^N$, the i th entry of \mathbf{u}_k^N , and $\bar{v}_k^N(c_{X,j}) = \sqrt{N/L} v_{k,j}^N$, the j th entry of \mathbf{v}_k^N . The off-grid values of $\bar{u}_k^N(y)$ and $\bar{v}_k^N(x)$ are obtained through linear interpolation. Then, we can show the following property.

Proposition 1 (Symmetry Property). *Suppose that there exist squared-integrable functions $w_{k,1}(y)$ and $w_{k,2}(x)$, such that $\bar{u}_k^N(y)$ and $\bar{v}_k^N(x)$ uniformly converge to $w_{k,1}(y)$ and $w_{k,2}(x)$, respectively, as $N \rightarrow \infty$. Then, $w_{k,1}(y)$ and $w_{k,2}(x)$ can be expressed as $w_{k,1}(y) = w(y - s_{k,2})$ and $w_{k,2}(x) = w(y - s_{k,1})$, where $w(x)$ is a symmetric, unimodal, non-negative function with $w(-x) = w(x)$, and $\int_{-\infty}^{\infty} w(x)^2 dx = 1$.*

Proof. See Appendix B. \square

Proposition 1 suggests a method to find the peaks of the signature vectors \mathbf{u}_k and \mathbf{v}_k using the symmetry property.

C. A Location Estimator

We first establish a general property of a unimodal symmetric function $w(x)$.

Lemma 1 (Monotone property). *Suppose that the non-negative function $w(x)$ is unimodal and symmetric about $x = 0$. Then, the autocorrelation function*

$$\tau(t) = \int_{-\infty}^{\infty} w(x)w(x-t)dx \quad (8)$$

is non-negative and symmetric about $t = 0$. In addition, $\tau(t)$ is strictly decreasing in $t > 0$.

Proof. The result can be easily derived using the unimodal and symmetry property of $w(x)$. The details are omitted here due to page limit. \square

From Lemma 1, $\tau(t)$ is maximized as $t = 0$. As a result, the non-negative, unimodal, and symmetric function $w(y - s_{1,1})$ from Proposition 1 has the following autocorrelation function

$$\int_{-\infty}^{\infty} w(y - s_{1,1})w(-y + t - s_{1,1})dy \quad (9)$$

$$= \int_{-\infty}^{\infty} w(y - s_{1,1})w(y - t + s_{1,1})dy \quad (10)$$

$$= \int_{-\infty}^{\infty} w(z)w(z + 2s_{1,1} - t)dz \quad (11)$$

$$= \tau(t - 2s_{1,1})$$

which is maximized at $t = 2s_{1,1}$, where the first equality (10) is due to symmetry $w(y) = w(-y)$, and the second equality (11) is from the change of variable $z = y - s_{1,1}$.

Given a vector $\mathbf{v} \in \mathbb{R}^N$ and the corresponding N -point coordinates $\mathbf{c}_X = [c_{X,1}, c_{X,2}, \dots, c_{X,N}]$, let $\bar{v}(x)$ be an interpolation function such that $\bar{v}(x) = \sqrt{N/L} v_i$ for $x = c_{X,i}$, $1 \leq i \leq N$, and $\bar{v}(x)$ is equivalent to a linear interpolation at off-grid locations. Define the reflected correlation function as

$$R(t; \mathbf{v}, \mathbf{c}_X) = \int_{-\infty}^{\infty} \bar{v}(x)\bar{v}(-x + t)dx. \quad (12)$$

Then, an estimate of the point of symmetry for \mathbf{v} in a continuous interval can be obtained as

$$\hat{s}(\mathbf{v}) = \frac{1}{2} \operatorname{argmax}_{t \in \mathbb{R}} R(t; \mathbf{v}, \mathbf{c}_X). \quad (13)$$

Note that, the estimator (13) aggregates the contributions from all measurements, including those far away from the source.

As a result, if one can obtain estimates $\hat{\mathbf{u}}_k$ and $\hat{\mathbf{v}}_k$ of the signature vectors \mathbf{u}_k and \mathbf{v}_k from the observation matrix \mathbf{H} , the estimate of the k th the source location can be computed as $\hat{\mathbf{s}}_k = (\hat{\mathbf{s}}(\hat{\mathbf{v}}_k), \hat{\mathbf{s}}(\hat{\mathbf{u}}_k))$ according to the symmetry property in Proposition 1.

D. Problem Formulation for Extracting Signature Vectors

There are two remaining issues: First, one needs to extract K pairs of signature vectors from the incomplete noisy observation matrix \mathbf{H} . Second, one needs to find the best coordinate system \mathcal{C} for grid points $c_X \times c_Y$ that define the observation matrix $\mathbf{H} = \mathbf{H}(\theta)$, since $\mathbf{H}(\theta)$ is variant according to the rotation θ of the coordinate system.

We answer these two questions by proposing a *UMF* problem specified as follows.

Denote by \mathcal{U}_s^N the cone specified by the unimodal constraints (6)–(7) for a fixed s . Denote $\mathcal{U}^N = \bigcup_{s=1}^N \mathcal{U}_s^N$ as the non-negative unimodal cone, and $\mathcal{U}^{N \times K}$ as the set of $N \times K$ real matrices where all the columns are in \mathcal{U}^N . Let $\mathbf{U}, \mathbf{V} \in \mathbb{R}^{N \times K}$ be the matrices that each contains K pairs of signature vectors $\{\mathbf{u}_k, \mathbf{v}_k\}$ to be determined. Let $\mathbf{W} \in \mathbb{R}^{N \times N}$ be an indicator matrix that describes the sampling strategy, where $W_{ij} = 1$, if $(i, j) \in \Omega$, and $W_{ij} = 0$, otherwise, where Ω denotes the set of entries that are assigned values based on (2), $|\Omega| = M$.

The source signature vectors can be extracted as the solution to the following problem:

$$\mathcal{P}1: \quad \underset{\mathbf{U}, \mathbf{V}}{\text{minimize}} \quad \|\mathbf{W} \odot (\mathbf{H} - \mathbf{U}\mathbf{V}^T)\|_F^2 \quad (14)$$

$$\text{subject to} \quad \mathbf{U} \in \mathcal{U}^{N \times K}, \mathbf{V} \in \mathcal{U}^{N \times K} \quad (15)$$

where \odot denotes the Hadamard product, i.e., $\mathbf{W} \odot \mathbf{H}$ is an $N \times N$ matrix computed entry-by-entry with $[\mathbf{W} \odot \mathbf{H}]_{ij} = W_{ij}H_{ij}$.

In the remaining part of this paper, we will discuss the cases of single source, two sources, and arbitrary number of sources, and the corresponding methods to solve $\mathcal{P}1$ or relaxed versions of it.

IV. SPECIAL CASE I: SINGLE SOURCE

In the single source case, we first show that a relaxation of $\mathcal{P}1$ can be easily solved by a matrix completion problem followed by SVD. We then analyze the squared error bound of the source localization.

A. Solution via Nuclear Norm Minimization

Dropping the unimodal constraints (15) and applying a convex relaxation on the objective function, $\mathcal{P}1$ can be relaxed to a classical rank- K matrix completion problem via nuclear norm minimization. It has been shown in the sparse signal processing literature that, under some mild regularization conditions on the low rank matrix \mathbf{H} , the matrix \mathbf{H} can be recovered, with a high probability, from the sparse and noisy

observation $\mathbf{W} \odot \mathbf{H}$ [20], [21]. Specifically, the noisy recovery of \mathbf{H} can be obtained as a solution, $\hat{\mathbf{X}}$, to the following convex optimization problem [18], [21]:

$$\begin{aligned} \mathcal{P}2: \quad & \underset{\mathbf{X}}{\text{minimize}} \quad \|\mathbf{X}\|_* \\ & \text{subject to} \quad \sum_{(i,j) \in \Omega} |X_{ij} - H_{ij}|^2 \leq \epsilon^2 \end{aligned} \quad (16)$$

where $\|\mathbf{X}\|_*$ denotes the nuclear norm of \mathbf{X} (i.e., the sum of the singular values of \mathbf{X}), and ϵ^2 is a small parameter (depending on the observation noise [21]) for the tolerance of the observation noise in \mathbf{H} .

Note that under exact recovery $\hat{\mathbf{X}} = \mathbf{H}$, the signature vectors are exactly the dominant singular vectors of \mathbf{X} , and the unimodal constraints (15) are then automatically satisfied. As a result, an efficient approximate solution to $\mathcal{P}1$ can be obtained from the dominant singular vectors $\hat{\mathbf{u}}_1$ and $\hat{\mathbf{v}}_1$ of $\hat{\mathbf{X}}$ as the solution to $\mathcal{P}2$.

B. Squared Error Bound

Let $\mathbf{e}_1^N = \hat{\mathbf{v}}_1^N - \mathbf{v}_1^N$ be the error vector, where the superscript N explicitly indicates that the analysis is performed under an $N \times N$ grid topology. Let $\bar{v}_1^N(x)$ be the linear interpolation function of $\hat{\mathbf{v}}_1^N$ attached with coordinates \mathbf{c}_X^N . Define $\bar{e}_1^N(x) = \bar{v}_1^N(x) - w_1(x)$ where $w_1(x) \triangleq w(x - s_{1,1})$ is the limiting function defined in Proposition 1. Define $E^N(s) \triangleq \int_{-\infty}^{\infty} \bar{e}_1^N(x) \bar{e}_1^N(-x + s) dx$. Suppose that the following regularity conditions are satisfied

$$\limsup_{N \rightarrow \infty} \frac{\left| \int_{-\infty}^{\infty} w_1(x) \bar{e}_1^N(-x + s) dx \right|}{|(\mathbf{v}_1^N)^T \mathbf{e}_1^N|} \leq \frac{C_e}{2} < \infty \quad (17)$$

$$\lim_{N \rightarrow \infty} \frac{E^N(s)}{|(\mathbf{v}_1^N)^T \mathbf{e}_1^N|} = 0 \quad (18)$$

with probability 1, for any $-\frac{L}{2} \leq s \leq \frac{L}{2}$ and any rotation of the coordinate system \mathcal{C} .

Remark 1 (Interpretation of (17)–(18)). The value C_e depends on the distributions of the sample locations and sample noise, as well as the energy field function $h(d)$. An intuitive explanation of the boundedness of C_e and the diminishing value of $E^N(s)/|(\mathbf{v}_1^N)^T \mathbf{e}_1^N|$ as $N \rightarrow \infty$ is that the observation noise is uncorrelated and identically distributed if sampled at the opposite locations symmetric about the source. For example, in our numerical experiment using uniformly random sampling corrupted by Gaussian noise in an underwater acoustic environment (see Section VII for the empirical propagation model), properties (17)–(18) are observed.

In addition, let $\kappa^N = (\sigma_{k,1}^N - \sigma_{k,2}^N)/\alpha_1$ be the normalized singular value gap from the model (5) for the single source $k = 1$, and suppose that the gap is non-diminishing, i.e., $\kappa \triangleq \liminf_{N \rightarrow \infty} \kappa^N > 0$. Furthermore, suppose that for the autocorrelation function $\tau(t)$, the first and the second-order derivatives, $\tau'(t)$ and $\tau''(t)$, exist and are continuous at $t = 0$. Then, for a small $\nu > 0$, there exists $a_\nu > 0$, such that $\tau(t) \leq \tau(0) + \tau'(0)t + \frac{1}{2}(\tau''(0) + \nu)t^2$ for all $t \in [0, a_\nu]$. We have the following theorems to characterize the asymptotic behavior of the squared estimation error $\|\hat{\mathbf{s}}_1 - \mathbf{s}_1\|_2^2$.

1) *Conservative construction*: Choose $N = \sqrt{M}$ and suppose that all the entries of \mathbf{H} are observed. As a result, the signature vectors $\hat{\mathbf{u}}_1$ and $\hat{\mathbf{v}}_1$ can be directly extracted as the dominant left and right singular vectors of \mathbf{H} .

Theorem 2 (Squared Error Bound under the Conservative Construction). *Under the condition of Proposition 1, for asymptotically large M ,*

$$\|\hat{\mathbf{s}}_1 - \mathbf{s}_1\|_2^2 \leq C_1 \frac{L^4}{M^{1.5}} + C_2 \frac{L^2}{\sqrt{M}} \frac{\bar{\sigma}_n^2}{\alpha_1^2} \quad (19)$$

with probability at least $1 - 2e^{-C_3 N}$, where $C_1 = \frac{3C_0 C_e K_h^2}{-\kappa^2(\tau''(0)+\nu)}$, $C_2 = \frac{6C_0 C_e}{-\kappa^2(\tau''(0)+\nu)}$, K_h is the Lipschitz parameter of $h(d)$, and C_0 and C_3 are constants.

Proof. See Appendix C. \square

Remark 2. The constants C_1 and C_2 show that the energy decay rate of $h(d)$ versus d may play a complicated role in the localization performance. A large decay rate, corresponding to a large Lipschitz parameter K_h , may harm the performance, because it leads to high discretization error. On the other hand, a small decay rate for $h(d)$ may result in performance less tolerant to noise, because the autocorrelation function $\tau(t)$ is less sharp. The key message of Theorem 2 is to establish the worst case performance scaling law, which will be discussed later.

2) *Aggressive construction*: Choose the number of sensors M and the matrix dimension N , such that M is the smallest integer that satisfies $M \geq CN(\log N)^2$. The signature vectors $\hat{\mathbf{u}}_1$ and $\hat{\mathbf{v}}_1$ are extracted from $\hat{\mathbf{X}}$, the solution to $\mathcal{P}2$.

Theorem 3 (Squared Error Bound under the Aggressive Construction). *Suppose that the sampling error of \mathbf{H} is bounded as $\sum_{(i,j)} |H_{ij} - \hat{H}_{ij}|^2 \leq \epsilon^2$, where ϵ is the parameter used in $\mathcal{P}2$. Then, under the condition of Proposition 1, there exists some $0 < \alpha < \frac{1}{2}$, such that for asymptotically large M and high enough signal-to-noise ratio (SNR) $\alpha_1/\bar{\sigma}_n^2$,*

$$\|\hat{\mathbf{s}}_1 - \mathbf{s}_1\|_2^2 \leq C_3 \frac{L^4}{M^{2-\alpha}} + C_4 \frac{L^3}{M^{1-\alpha}} \frac{\bar{\sigma}_n}{\alpha_1} + C_5 L^2 \frac{\bar{\sigma}_n^2}{\alpha_1^2} \quad (20)$$

with probability $1 - \mathcal{O}(N^{-\beta})$, where $C_3 = \frac{C'_0 C_e K_h^2}{-2\kappa^2(\tau''(0)+\nu)}$, $C_4 = \frac{\sqrt{2}C'_0 C_e K_h}{-\kappa^2(\tau''(0)+\nu)}$, $C_5 = \frac{C'_0 C_e}{-\kappa^2(\tau''(0)+\nu)}$, and C'_0 and β are constants.

Proof. See Appendix C. \square

3) *Discussions*: We draw the following observations.

Performance Scaling Law: Theorems 2 and 3 reveal the error exponent as the number of sensors increases. As a performance benchmark, for a naive non-parametric peak localization scheme that estimates the source location directly from the position of the measurement sample that achieves the highest energy, the localization squared error decreases as $\mathcal{O}(1/M)$, whereas, the squared error of the proposed schemes decreases faster than $\mathcal{O}(1/M^{1.5})$ in high SNR $\alpha_1/\bar{\sigma}_n^2 \gg 1$, order-wise faster than the naive scheme, as will be demonstrated by our numerical results in Section VII.

Sparsity and Noise Suppression Tradeoff: While the aggressive construction strategy achieves higher error decay

rate in terms of the number of samples M under high SNR $\triangleq \alpha_1/\bar{\sigma}_n^2 \gg 1$, the aggressive construction scheme is less tolerant to measurement noise as observed from the last terms in (19) and (20). Specifically, in low SNR, the squared error bound of the aggressive construction strategy scales as $\mathcal{O}(\frac{1}{\text{SNR}})$, whereas, it scales as $\mathcal{O}(\frac{1}{N\text{SNR}})$ for the conservative construction strategy.

Impact from the Propagation Law: The parameter $0 < \kappa \leq 1$, as appear in the coefficients of the bound, captures how precisely the outer product $\mathbf{u}_k \mathbf{v}_k^T$ of the signature vectors may approximate the energy field matrix $\mathbf{H}^{(k)}$ for a single source. In the special case when $h(d)$ is fully decomposable, i.e., $h(d(x, y)) = h_1(x)h_2(y)$, we have $\kappa = 1$ leading to a small error bound.¹ For most practical propagation models we have tested (e.g., propagations of radio signals over the air, acoustic signals in the water, etc.), κ is close to 1.

V. SPECIAL CASE II: TWO SOURCES

In the case of two sources, the SVD may not extract the desired signature vectors from \mathbf{H} in (5), because the signature vectors \mathbf{u}_1 and \mathbf{u}_2 from different sources are not necessarily orthogonal. However, it turns out that by choosing an appropriate coordinate system \mathcal{C} , the corresponding UMF problem $\mathcal{P}1$ can be easily solved (under some mild conditions). In this section, we propose rotation techniques to select the best coordinate system for extracting the source signature vectors.

A. Optimal Rotation of the Coordinate System

Suppose that we fix the origin at the center of the target area and rotate the coordinate system such that the two sources are aligned, without loss of generality (w.l.o.g.), on the y axis. Then, the source locations satisfy $s_{1,1} = s_{2,1}$, and the signature vectors follow $\mathbf{v}_1 = \mathbf{v}_2$. This approximately yields a rank-1 model $\mathbf{H} = \mathbf{H}^{(1)} + \mathbf{H}^{(2)} \approx (\alpha_1 \mathbf{u}_1 + \alpha_2 \mathbf{u}_2) \mathbf{v}_1^T$ by ignoring the minor components in (5).

As a result, an algorithm can be designed as follows. First, extract the vectors $\hat{\alpha}_1 \hat{\mathbf{u}}_1 + \hat{\alpha}_2 \hat{\mathbf{u}}_2$ and $\hat{\mathbf{v}}_1$ by solving the matrix completion problem $\mathcal{P}2$ followed by the SVD as developed in Section IV. Second, obtain $\hat{\mathbf{u}}_1$ and $\hat{\mathbf{u}}_2$ from the composite vector $\hat{\alpha}_1 \hat{\mathbf{u}}_1 + \hat{\alpha}_2 \hat{\mathbf{u}}_2$.

The remaining challenge is to find optimal rotated coordinate system for source alignment from the M measurement samples. Note that the source topology is not known.

Denote $\mathbf{H}(\theta)$ as the observation matrix constructed in coordinate system \mathcal{C}_θ with θ degrees of rotation to reference coordinate system \mathcal{C} . The desired rotation θ can be obtained as

$$\mathcal{P}3: \quad \underset{\theta \in [0, \frac{\pi}{2}]}{\text{maximize}} \quad \rho(\theta) \triangleq \frac{\sigma_1^2(\mathbf{H}(\theta))}{\sum_{k=1}^N \sigma_k^2(\mathbf{H}(\theta))} \quad (21)$$

where $\sigma_k(\mathbf{H})$ is defined as the k th largest singular value of $\hat{\mathbf{X}}(\mathbf{H})$, the solution to the matrix completion problem $\mathcal{P}2$ based on \mathbf{H} .

Note that $\rho(\theta) \leq 1$ for all $\theta \in [0, \frac{\pi}{2}]$. In addition, $\rho(\theta^*) = 1$, when $\mathbf{H}(\theta)$ becomes a rank-1 matrix where the sources

¹The only example for this special case is the Gaussian function, i.e., $h(d(x, y)) = ae^{-b(x^2+y^2)} = ae^{-bx^2} e^{-by^2}$.

are aligned with one of the axes, which gives an intuitive justification for $\mathcal{P}3$.

However, an exhaustive search for the solution θ^* is computationally expensive, since it requires performing SVD on $\mathbf{H}(\theta)$ for each θ . Yet, it can be shown that $\rho(\theta)$ has a nice locally unimodal property that enables an efficient solution.

Let $\mathbf{H}(\theta)$ be the signature matrix defined in (5) under the coordinate system \mathcal{C}_θ .

Theorem 4 (Property of $\rho(\theta)$). *Assume that the two sources have equal transmission power $\alpha_1 = \alpha_2$. In addition, suppose that $\mathbf{H}(\theta)$ is at most rank-2 and can be perfectly recovered from $\mathbf{H}(\theta)$, i.e., $\hat{\mathbf{X}}(\mathbf{H}(\theta)) = \mathbf{H}(\theta)$. Consider that N is large enough. Then, $\rho(\theta)$ is periodic, i.e., $\rho(\theta) = \rho(\theta + \frac{\pi}{2})$. In addition, $\rho(\theta)$ is strictly increasing over $(\theta^* - \frac{\pi}{4}, \theta^*)$ and strictly decreasing over $(\theta^*, \theta^* + \frac{\pi}{4})$, if the energy field satisfies*

$$s \cdot \tau'(t) > t \cdot \tau'(s) \quad (22)$$

for all $0 < s < t$, where $\tau'(t) \triangleq \frac{d}{dt}\tau(t)$ and θ^* is the maximizer of $\rho(\theta)$.

Proof. See Appendix D. \square

The result in Theorem 4 confirms that the function $\rho(\theta)$ has a unique local maximum within a $\frac{\pi}{2}$ -window under a mild condition, in the ideal case of perfect recovery $\hat{\mathbf{X}}(\mathbf{H}(\theta)) = \mathbf{H}(\theta)$. The property motivates a simple bisection search algorithm to efficiently search for the globally optimal solution, θ^* , to $\mathcal{P}3$.

Note that condition (22) can be satisfied by a variety of energy fields. For example, for Laplacian field $h(x, y) = \gamma e^{-\gamma|x| - \gamma|y|}$, we have the autocorrelation function $\tau(t) = (1 + \gamma t)e^{-\gamma t}$, and its derivative $\tau'(t) = -\gamma^2 t e^{-\gamma t}$; for Gaussian field $h(d) = \sqrt{2\gamma/\pi} e^{-\gamma d^2}$, where $d^2 = x^2 + y^2$, we have $\tau(t) = e^{-\gamma t^2/2}$, and $\tau'(t) = -\gamma t e^{-\gamma t^2/2}$. In both cases, condition (22) is satisfied.

B. Source Separation

W.l.o.g., suppose that the signature matrix has a decomposition form $\mathbf{H} \approx (\alpha_1 \mathbf{u}_1 + \alpha_2 \mathbf{u}_2) \mathbf{v}_1^T$ after the optimal coordinate system rotation from solving $\mathcal{P}3$. In addition, assume the equal power case $\alpha_1 = \alpha_2$. Then, using a technique similar to that in Section IV, we can estimate the x coordinates from

$$\hat{s}_{1,1} = \hat{s}_{2,1} = \frac{1}{2} \operatorname{argmax}_{t \in \mathbb{R}} R(t; \hat{\mathbf{v}}_1, \mathbf{c}_X). \quad (23)$$

In addition, the y coordinates can be estimated as $\hat{s}_{1,2}, \hat{s}_{2,2} = \hat{c} \pm r$, where

$$\hat{c} = \frac{1}{2} \operatorname{argmax}_{t \in \mathbb{R}} R(t; \hat{\mathbf{u}}_1, \mathbf{c}_Y), \quad \hat{r} = \operatorname{argmax}_{r \geq 0} Q(r; \hat{\mathbf{u}}_1, \hat{\mathbf{v}}_1) \quad (24)$$

and

$$Q(r; \hat{\mathbf{u}}_1, \hat{\mathbf{v}}_1) \triangleq \frac{1}{2} \int_{-\infty}^{\infty} \hat{u}(x) \left(\hat{v}(x - \hat{c} - r) + \hat{v}(x - \hat{c} + r) \right) dx$$

in which, $\hat{u}(x)$ is a linear interpolation of $\hat{\mathbf{u}}_1$ (similar to $\bar{v}(x)$ in (12)) and $\hat{v}(x)$ is from linearly interpolating $\hat{\mathbf{v}}_1$. Using calculations similar to (9)–(11), it can be shown that $Q(r; \mathbf{u}_1 + \mathbf{u}_2, \mathbf{v}_1)$ is maximized at $r^* = (s_{1,2} - s_{2,2})/2$ if the

interpolation is perfect, i.e., $\hat{u}(x) = w(x - s_{1,2}) + w(x - s_{2,2})$ and $\hat{v}(x - s_{1,1}) = w(x - s_{1,1})$.

As a remark, a simple peak finding solution may not work as well as the estimator from (23)–(24) because, first, peak finding mostly depends on the measurement around the centroid \hat{c} and the information from other measurements may not be fully exploited, and second, when two sources are close to each other, their aggregate energy field will appear as one peak, which does not correspond to the desired source location. On the other hand, the proposed procedure (23)–(24) can resolve these issues.

VI. GENERAL CASE: ARBITRARY NUMBER OF SOURCES

In the case of an arbitrary number of sources, we first study a general algorithm framework to solve $\mathcal{P}1$. We then discuss efficient approximations for fast implementation of the algorithm. Finally, an optimization of the coordinate system \mathcal{C}_θ is studied to enhance the convergence of the algorithm.

A. The Gradient Projection

Let $f(\mathbf{U}, \mathbf{V}) = \|\mathbf{W} \odot (\mathbf{H} - \mathbf{U}\mathbf{V}^T)\|_F^2$. With some algebra and matrix calculus, it can be shown that the gradients of f are

$$\frac{\partial}{\partial \mathbf{U}} f = -2(\mathbf{W} \odot \mathbf{H})\mathbf{V} + 2(\mathbf{W} \odot (\mathbf{U}\mathbf{V}^T))\mathbf{V}$$

$$\frac{\partial}{\partial \mathbf{V}} f = -2(\mathbf{W}^T \odot \mathbf{H}^T)\mathbf{U} + 2(\mathbf{W}^T \odot (\mathbf{V}\mathbf{U}^T))\mathbf{U}$$

and the iteration of the projected gradient algorithm can be computed as

$$\mathbf{U}(t+1) = \mathcal{P}_U \left\{ \mathbf{U}(t) - \mu_t \frac{\partial}{\partial \mathbf{U}} f(\mathbf{U}(t), \mathbf{V}(t)) \right\} \quad (25)$$

$$\mathbf{V}(t+1) = \mathcal{P}_V \left\{ \mathbf{V}(t) - \nu_t \frac{\partial}{\partial \mathbf{V}} f(\mathbf{U}(t+1), \mathbf{V}(t)) \right\} \quad (26)$$

where $\mathcal{P}_U\{\cdot\}$ is a projection operator to project any $N \times K$ matrix onto the unimodal cone $\mathcal{U}^{N \times K}$, and the step size μ_t and ν_t are chosen to ensure the decrease of the objective function f (for example, via a backtracking line search [22], [23]).

B. Fast Unimodal Projection

The projection $\mathcal{P}_U\{\mathbf{X}\}$ onto the unimodal cone is formally defined as the solution that minimizes $\|\mathbf{X} - \mathbf{Y}\|_F$ over $\mathbf{Y} \in \mathcal{U}^{N \times K}$. Due to the property of the Frobenius norm, the projection can be computed column-by-column.

While it is not straight-forward to efficiently project onto the convex set \mathcal{U}_s^N (specified by constraints (6)–(7)) as it may seem to be, it is relatively easier to compute the projection onto an *isotonic cone*, where an isotonic sequence is defined as a non-increasing (or non-decreasing) sequence. Recently, a fast algorithm for exact isotonic projection was developed in [24], which finds the solution within $N - 1$ steps. With such a tool, a fast approximate algorithm to compute $\mathcal{P}_U\{\mathbf{X}\}$ can be described as follows.

Fast unimodal projection:

- 1) For each odd index s , compute the isotonic projection for \mathbf{x}_k , the k th column of \mathbf{X} , to form an ascending branch y_1, y_2, \dots, y_s and a descending branch

$y_{s+1}, y_{s+2}, \dots, y_N$, respectively, using the exact isotonic projection algorithm in [24].

- 2) Construct $\mathbf{y}^{(s)} := (y_1, y_2, \dots, y_s, y_{s+1}, \dots, y_N)$, and repeat from Step 1) to compute a series of projections $\mathbf{y}^{(s)}$ for $s = 1, 3, 5, \dots$.
- 3) Choose the solution $\mathbf{y}^{(s^*)}$ that minimizes $\|\mathbf{y}^{(s)} - \mathbf{x}_k\|$ over $s = 1, 3, 5, \dots$.

Since Step 1) has complexity at most N , the overall complexity is at most $\frac{1}{2}N^2$.

Note that minimizing $\|\mathbf{x} - \mathbf{y}\|_2^2$ subject to the unimodal constraint $\mathbf{y} \in \mathcal{U}^N = \bigcup_{s=1}^N \mathcal{U}_s^N$ is equivalent to solving a series of minimization problems, each under constraint $\mathbf{y} \in \mathcal{U}_s^N \cup \mathcal{U}_{s+1}^N$ for $s = 1, 3, 5, \dots$. In addition, each subproblem is equivalent to minimizing $\|\mathbf{x}_{1:s} - \mathbf{y}'\|_2^2 + \|\mathbf{x}_{s+1:N} - \mathbf{y}''\|_2^2$ subject to $0 \leq y'_1 \leq y'_2 \leq \dots \leq y'_s$ and $y''_1 \geq y''_2 \geq \dots \geq y''_{N-s}$, where $\mathbf{x}_{a:b} = (x_a, x_{a+1}, \dots, x_b)$ represents a vector that is extracted from the a th entry to the b th entry of \mathbf{x} . Therefore, the above unimodal projection is exact.

C. Local Convergence Analysis

We frame the analysis according to the following two observations. First, when there is no sampling noise, the unimodal constraint $(\mathbf{U}, \mathbf{V}) \in \mathcal{U}^{N \times K} \times \mathcal{U}^{N \times K}$ is not active at the globally optimal point $\hat{\mathbf{X}} = (\hat{\mathbf{U}}, \hat{\mathbf{V}})$. Then, we can remove the projection in (25) and (26) and analyze the local behavior of an unconstrained algorithm approaches $\hat{\mathbf{X}}$. The goal is to discover any factor that possibly harms the convergence and determines methods that will improve the performance.

Second, note that the function is bi-convex. Therefore, we can study partial convergence, where the convergence of the variable \mathbf{U} is analyzed while fixing the other variable \mathbf{V} to be in the neighborhood of $\hat{\mathbf{V}}$. As a result, the unconstrained algorithm trajectory for \mathbf{U} will converge to a unique solution. Analyzing the asymptotic convergence rate of \mathbf{U} may help us understand the factors that affect algorithm convergence.

Denote $g(\mathbf{X}) = [(\partial f / \partial \mathbf{U})^T (\partial f / \partial \mathbf{V})^T]^T$ as the gradient function of $f(\mathbf{X})$, where $\mathbf{X} = (\mathbf{U}, \mathbf{V})$. Suppose $\mathbf{X}(0)$ is sufficiently close to $\hat{\mathbf{X}}$, such that the unimodal constraints are not active. As a continuous counter-part to the discrete iteration (25)–(26), the continuous algorithm trajectory $\mathbf{X}(t)$ can be given as

$$\frac{d}{dt} \mathbf{X}(t) = -g(\mathbf{X}(t)). \quad (27)$$

Let $\mathcal{E}(\mathbf{X}_e(t)) = \frac{1}{2} \|\mathbf{X}_e(t)\|_F^2$ be the normed error function for the convergence error $\mathbf{X}_e(t) \triangleq \mathbf{X}(t) - \hat{\mathbf{X}}$. Let $\mathbf{U}_e = \mathbf{U} - \hat{\mathbf{U}}$ and $\mathbf{V}_e = \mathbf{V} - \hat{\mathbf{V}}$ with the time index t dropped for notational brevity. The following result suggests that if either \mathbf{U}_e or \mathbf{V}_e is much smaller than the other variable, then the algorithm trajectory $\mathbf{X}(t)$ converges exponentially to $\hat{\mathbf{X}}$.

Proposition 2 (Partial convergence). *Assume perfect sampling $\mathbf{H} = \mathbf{H}$ and \mathbf{H} in (5) has rank K . Suppose that the algorithm initialization $\mathbf{X}(0)$ is in the neighborhood of the optimal solution $\hat{\mathbf{X}}$ to $\mathcal{P}1$. Then the following holds*

$$\frac{d}{dt} \mathcal{E}(\mathbf{X}_e) \leq -2\lambda_K(\hat{\mathbf{V}}^T \hat{\mathbf{V}}) \|\mathbf{U}_e\|_F^2 + o(\|\mathbf{U}_e\|_F^2) \quad (28)$$

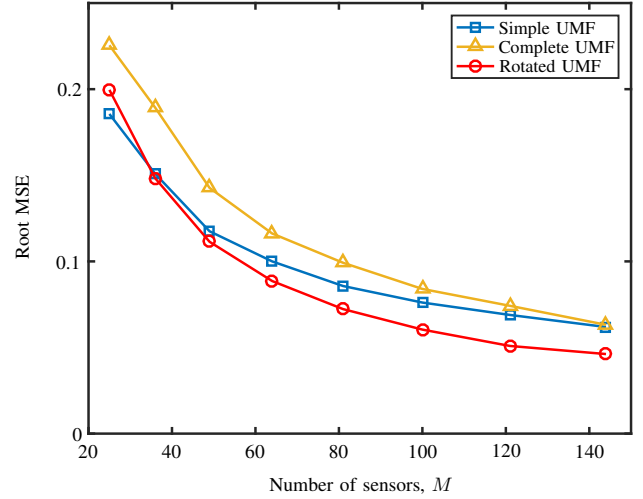


Figure 2. Localization performance under noise-free sampling in a two source Gaussian energy field.

for $\|\mathbf{V}_e\|_F = o(\|\mathbf{U}_e\|_F)$, where $\lambda_K(\mathbf{A})$ denotes the smallest eigenvalue of \mathbf{A} . Moreover,

$$\frac{d}{dt} \mathcal{E}(\mathbf{X}_e) \leq -2\lambda_K(\hat{\mathbf{U}}^T \hat{\mathbf{U}}) \|\mathbf{V}_e\|_F^2 + o(\|\mathbf{V}_e\|_F^2) \quad (29)$$

for $\|\mathbf{U}_e\|_F = o(\|\mathbf{V}_e\|_F)$.

Proof. See Appendix E. \square

Proposition 2 shows that the rate of convergence depends on the eigenvalues of $\hat{\mathbf{V}}^T \hat{\mathbf{V}}$ and $\hat{\mathbf{U}}^T \hat{\mathbf{U}}$, where $\hat{\mathbf{V}}$ and $\hat{\mathbf{U}}$ carry the location signatures of the source. Specifically, if the sources are aligned with either the x axis or the y axis, then either $\hat{\mathbf{U}}$ or $\hat{\mathbf{V}}$ tends to have identical columns, which leads to rank deficiency of matrices $\hat{\mathbf{U}}^T \hat{\mathbf{U}}$ or $\hat{\mathbf{V}}^T \hat{\mathbf{V}}$, corresponding to small eigenvalues λ_K and hence slow convergence. This result suggests gradient type algorithms work better when sources are well-separated on both axes.

D. Rotation for Convergence Improvement

According to Proposition 2, we may need to establish a coordinate system such that the sources are well separated on both axes. However, the challenge is that we have *no* prior knowledge of the source locations.

Recall that $\mathbf{H}(\theta)$ denotes the observation matrix constructed in coordinate system \mathcal{C}_θ with θ degrees of rotation with respect to the reference coordinate system \mathcal{C} . Similar to $\mathcal{P}3$, the desired rotation θ can be obtained as

$$\mathcal{P}4: \quad \underset{\theta \in [0, \frac{\pi}{2}]}{\text{minimize}} \quad \rho(\theta) \triangleq \frac{\sigma_1^2(\mathbf{H}(\theta))}{\sum_{k=1}^N \sigma_k^2(\mathbf{H}(\theta))} \quad (30)$$

where $\sigma_k(\mathbf{H})$ is defined as the k th largest singular value of $\hat{\mathbf{X}}(\mathbf{H})$, the solution to the matrix completion problem $\mathcal{P}2$ based on \mathbf{H} .

While problem $\mathcal{P}3$ is to align the sources with one of the axes, problem $\mathcal{P}4$ tries to avoid alignments with any axes.

Fig. 2 demonstrates the performance of the UMF with optimal coordinate system rotation under noise-free sampling

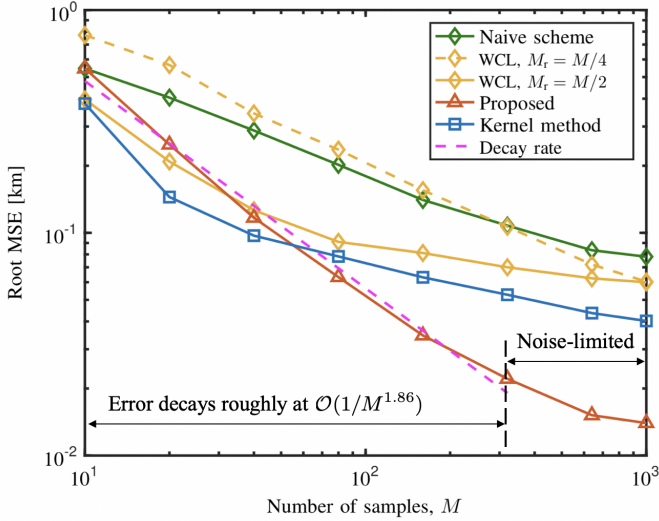


Figure 3. MSE of the source location versus the number of sensors, M , in the single source case.

$\sigma_n^2 = 0$, where $L = 1$ and the energy field is given by $h(d) = \sqrt{2\gamma/\pi} \exp(-\gamma d^2)$ with $\lambda = 20$. The observation matrices constructed with dimension N satisfy $N^2/2 \approx M$. There are two key observations: (i) the coordination system rotation does improve the convergence as demonstrated by the comparison between scheme “Rotated UMF”, which solves $\mathcal{P}1$ in the optimal coordinate system \mathcal{C}_{θ^*} with θ^* solved from $\mathcal{P}4$, and scheme “Simple UMF”, which solves $\mathcal{P}1$ in a fixed coordinate system \mathcal{C} . (ii) UMF performs better in the recovery of sparse unimodal structures as compared to conventional sparse matrix completion methods, scheme “Complete UMF”, which first solves the matrix completion problem $\mathcal{P}2$ in the optimal coordinate system \mathcal{C}_{θ^*} , and then solves $\mathcal{P}1$ for signature vector extraction. As the UMF is aware of the unimodal structure, the proposed “Rotated UMF” outperforms the “Complete UMF” scheme.²

VII. NUMERICAL RESULTS

We consider the source and sensor deployment model in Section II with $L = 5$ km in an underwater environment. The sources simultaneously transmit signals at $f = 5$ kHz. The propagation of the signal from each source is modeled using $N_p = 15$ discrete paths, where the path inter-arrival times $\tau_{p+1} - \tau_p$ are exponentially distributed with mean 100 ms, and the path amplitudes are Rayleigh distributed with power scaled as $e^{-\varphi(\tau_p - \tau_1)}$ with respect to the first path, $\varphi = 2 \text{ sec}^{-1}$ [25], [26]. The path energy attenuation is modeled as $(1 + d^{1.5} A(f)^d)^{-1}$, where Thorp’s formula [26] is used to arrive at $10 \log_{10} A(f) = 0.11 f^2 / (1 + f^2) + 44 f^2 / (4100 + f^2) + 2.75 \times 10^{-4} f^2 + 0.003$ dB/km. The ambient noise $n^{(m)}$ is modeled as a zero mean, Gaussian random variable with normalized variance $\sigma_n^2/P = -34$ dB, where $P = 1$ is the total transmission power. The sensor has a receive window of 4 seconds from the detection of the first path.

²However, we also note that in the case of low SNR, i.e., $\sigma_n^2 \gg 1$, $\mathcal{P}2$ can serve as an efficient de-noising step to help faster convergence of UMF.

The parameter N for constructing the observation matrix \mathbf{H} is chosen as the largest integer satisfying $1.5N(\log N)^2 \leq M$.

The proposed algorithms for the single source case ((13) in Section IV), two source ((23) – (24) in Section V), and an arbitrary number of sources (Section VI) is evaluated. Specifically, the projected gradient algorithm in (25)–(26) are initialized with random vectors (entries independently and uniformly distributed in $[0, 1]$) projected on the unimodal cone. The algorithm was run 5 times, each with independent initializations and a maximum of 200 iterations. The solution (out of the 5) that yields the smallest objective function value was selected.

Three baseline schemes are evaluated. Baseline 1, *Naive scheme for single source*: the location of the sensor that observes the highest energy is identified as the source location. Baseline 2, *Weighted centroid localization* [7]: the location estimate is updated by

$$\hat{\mathbf{s}}(n+1) = \frac{\sum_{m \in \mathcal{R}(\hat{\mathbf{s}}(n))} \varrho^{(m)} \mathbf{z}^{(m)}}{\sum_{m \in \mathcal{R}(\hat{\mathbf{s}}(n))} \varrho^{(m)}}$$

until convergence, where $\varrho^{(m)} = (h^{(m)})^2$ are the squared-weights and $\mathcal{R}(\mathbf{x})$ specifies a set of measurements that are taken within a radius r from location \mathbf{x} , in which, the radius r is at least $L/8$ or as large as to include exactly $M_r \in \{M/4, M/2\}$ measurements. Baseline 3, *Kernel regression*: The algorithm chooses parameters $\{\alpha_k, \hat{\mathbf{z}}_k\}$ and λ to minimize $\sum_m |h^{(m)} - \sum_{k=1}^K \alpha_k B(\mathbf{z}^{(m)}, \hat{\mathbf{z}}_k; \lambda)|^2$ based on the measurement $\{h^{(m)}, \mathbf{z}^{(m)}\}$, where two classes of kernel functions are considered, Gaussian kernel $B_G(\mathbf{z}, \hat{\mathbf{z}}_k; \lambda) = \exp(-\lambda \|\mathbf{z} - \hat{\mathbf{z}}_k\|^2)$ and Laplacian kernel $B_L(\mathbf{z}, \hat{\mathbf{z}}_k; \lambda) = \exp(-\lambda \|\mathbf{z} - \hat{\mathbf{z}}_k\|_1)$, in which, $\|\cdot\|_1$ denotes the L_1 norm. Such a least-squares problem is solved 5 times with randomized initializations. Cross-validation is used to choose the best kernel function, and the data set is partitioned to 70% for parameter training and 30% for MSE performance validation. The parameters $\hat{\mathbf{z}}_k$ give the location estimates. Note that Baselines 1 and 2 cannot differentiate multiple sources when the two sources are close to each other. Therefore, these two baselines are evaluated in the single source case only.

Fig. 3 shows the rooted mean squared error (RMSE) of the source location versus the number of sensors, M , in the single source case. The proposed scheme outperforms the naive scheme and the weighted centroid scheme.³ It also outperforms the kernel method from moderate to large number of sensors. The dashed line with slope -0.93 shows that the error decay rate of the proposed algorithm in the $M = 10$ to 500 region is roughly $\mathcal{O}(1/M^{1.86})$. Note that Theorem 2 and 3 show that the MSE of the proposed scheme should decrease faster than $\mathcal{O}(1/M^{1.5})$, and hence is confirmed by our numerical results. In the case of more than 500 sensors, the error decay rate is limited by the ambient noise. This phenomenon also matches with the second and third terms of (20) in Theorem 3.

³It is observed from our numerical experiments that the weights ϱ and the window \mathcal{R} in the weighted centroid scheme should depend on M and $h(d)$. However, choosing the best weights and window are highly non-trivial.

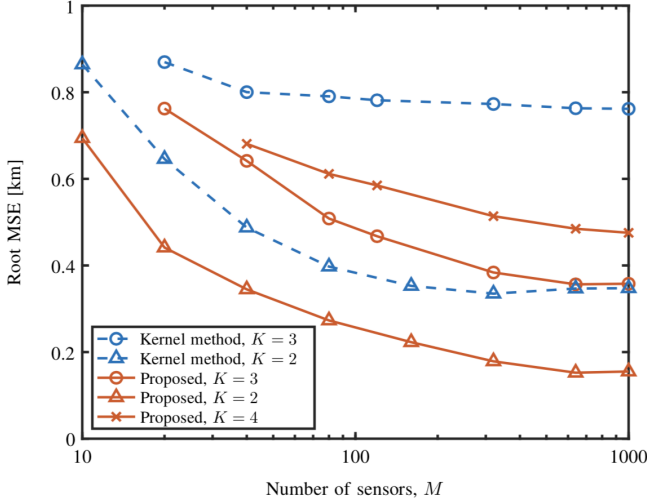


Figure 4. MSE of the source location versus the number of sensors, M , in two to four source cases.

Fig. 4 shows the RMSE of the source locations versus the number of sensors, M , in two to four source cases. The proposed methods significantly outperform the kernel methods. Note that the proposed schemes only require the generic property that the source energy field $h(d)$ is non-negative and strictly decreasing in the distance d to the source. Although the kernel functions also capture such property, the kernel methods suffer from parameter estimation error when fitting the data to inaccurate parametric models.

VIII. CONCLUSIONS

This paper developed non-parametric algorithms for localizing multiple sources based on a moderate number of energy measurements from different locations. A matrix observation model was proposed and it is proven that the dominant singular vectors of the matrix for a single source are unimodal and symmetric. A non-parametric source localization algorithm exploiting the unimodal and symmetry property was developed and shown to decrease the localization MSE faster than $\mathcal{O}(1/M^{1.5})$ using M sensors in the single source case with noiseless measurements. In the two source case, the source locations can be found by choosing the optimal rotation of the coordinate system such that the normalized dominant singular value of the sample matrix is maximized. In the case of arbitrary number of sources, we localize the sources by solving a UMF problem in an optimally rotated coordinate system. Our numerical experiments demonstrate that the proposed scheme achieves similar performance as the baselines using no more than $1/5$ measurement samples.

APPENDIX A PROOF OF THEOREM 1

As the signature vectors \mathbf{u}_k and \mathbf{v}_k correspond to the dominant singular vectors $\mathbf{u}_{k,1}$ and $\mathbf{v}_{k,1}$ of $\mathbf{H}^{(k)}$, we can focus on only one source and drop the source index k here for brevity. Specifically, from (5), we write $\mathbf{H} = \alpha \mathbf{u} \mathbf{v}^T + \sum_{i=2}^N \lambda_i \mathbf{u}_i \mathbf{v}_i^T$ (for the k th source, where $k = 1$), in which \mathbf{u} and \mathbf{u}_i

are the left singular vectors of \mathbf{H} , \mathbf{v} and \mathbf{v}_i are the right singular vectors, and α is the largest singular value, $\alpha > \lambda_i$, $i = 2, 3, \dots, N$.

Let $\mathbf{R} = \mathbf{H}^T \mathbf{H}$. Then, the (i, j) th entry of \mathbf{R} is given by $R_{ij} = \mathbf{h}_i^T \mathbf{h}_j$, where \mathbf{h}_i is the i th column of \mathbf{H} . In the following lemma, we show that the columns of \mathbf{R} are unimodal.

Lemma 2. Suppose that the source is located at the (m, n) th grid cell centered at $\mathbf{c}_{m,n}$. Then, for each column of \mathbf{R} , the entries R_{ij} are increasing, $R_{ij} < R_{i+1,j}$, if $i < n$, and they are decreasing, $R_{ij} > R_{i+1,j}$, if $i \geq n$.

Proof. Since the source location \mathbf{s} is inside the (m, n) th grid cell centered at $\mathbf{c}_{m,n}$, we have $d(\mathbf{c}_{p,i}, \mathbf{s}) > d(\mathbf{c}_{p,i+1}, \mathbf{s}) \geq d(\mathbf{c}_{p,n}, \mathbf{s})$, for $i < n$ and all $p = 1, 2, \dots, N$. Similarly, $d(\mathbf{c}_{p,i}, \mathbf{s}) < d(\mathbf{c}_{p,i+1}, \mathbf{s})$, for $i \geq n$ and all p . Recall that $H_{ij} = h(d(\mathbf{c}_{i,j}, \mathbf{s}))$ and $h(d)$ is a non-negative decreasing function. We thus have

$$\begin{aligned} R_{ij} &= \mathbf{h}_i^T \mathbf{h}_j = \sum_{p=1}^N H_{pi} H_{pj} \\ &< \sum_{p=1}^N H_{p,i+1} H_{pj} = \mathbf{h}_{i+1}^T \mathbf{h}_j = R_{i+1,j} \end{aligned}$$

for $i < n$. Similarly, we can show that $R_{ij} = \mathbf{h}_i^T \mathbf{h}_j > \mathbf{h}_{i+1}^T \mathbf{h}_j = R_{i+1,j}$, for $i \geq n$. \square

Under the condition of Lemma 2, if we raise \mathbf{R} to the power of q , the columns of \mathbf{R}^q are unimodal, with their peaks at the n th entry. Specifically, define $\mathbf{R}^{(q)} \triangleq \mathbf{R}^q / \text{tr}\{\mathbf{R}^q\}$. We show, in the following lemma, that the columns of $\mathbf{R}^{(q)}$ are unimodal.

Lemma 3. Let $R_{ij}^{(q)}$ be the (i, j) th entry of $\mathbf{R}^{(q)}$. Then, $R_{ij}^{(q)} < R_{i+1,j}^{(q)}$, if $i < n$, and $R_{ij}^{(q)} > R_{i+1,j}^{(q)}$, if $i \geq n$.

Proof. First, it can be easily verified that the result holds for $q = 1$ according to Lemma 2. Then, suppose that the result holds for some $q \geq 1$. Note that $\mathbf{R}^{(q+1)} = \text{tr}\{\mathbf{R}^{(q)}\} \mathbf{R}^{(q)} / \text{tr}\{\mathbf{R}^{(q+1)}\}$ and that $\mathbf{R}^{(q)}$ is symmetric. We have

$$\begin{aligned} R_{ij}^{(q+1)} &= \frac{\text{tr}\{\mathbf{R}^q\}}{\text{tr}\{\mathbf{R}^{q+1}\}} \sum_{p=1}^N R_{pi}^{(q)} R_{pj} \\ &< \frac{\text{tr}\{\mathbf{R}^q\}}{\text{tr}\{\mathbf{R}^{q+1}\}} \sum_{p=1}^N R_{p,i+1}^{(q)} R_{pj} = R_{i+1,j}^{(q+1)} \end{aligned}$$

for $i < n$. Similarly, we can show that $R_{ij}^{(q+1)} > R_{i+1,j}^{(q+1)}$, for $i \geq n$. Therefore, by deduction, the result holds for all $q \geq 1$. \square

Let $\mathbf{R}^\infty \triangleq \lim_{q \rightarrow \infty} \mathbf{R}^q / \text{tr}\{\mathbf{R}^q\}$. It can be shown that the limit exists and equals $\mathbf{R}^\infty = \mathbf{v} \mathbf{v}^T$. To see this, we can easily compute $\mathbf{R}^q = \alpha^{2q} \mathbf{v} \mathbf{v}^T + \sum_{i=2}^N \lambda_i^{2q} \mathbf{v}_i \mathbf{v}_i^T$ and the normalization term $\text{tr}\{\mathbf{R}^q\} = (\alpha^{2q} + \sum_{i=2}^N \lambda_i^{2q})$. By the Perron-Frobenius theorem, the dominant eigenvalue of a non-negative matrix has multiplicity 1, i.e., $\alpha = \lambda_1 > |\lambda_i|$ for all $i \geq 2$. Hence, $(\lambda_i/\alpha)^{2q} \rightarrow 0$ as $q \rightarrow \infty$, for $i = 2, 3, \dots, N$, leading to \mathbf{R}^∞ being rank-1.

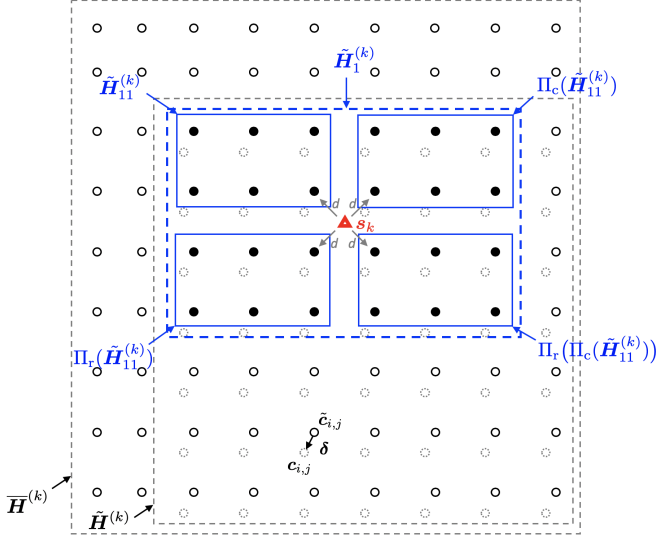


Figure 5. Construction of sub-blocks of $\tilde{\mathbf{H}}^{(k)}$ for the proof of Proposition 1.

On the other hand, from Lemma 3, each column of \mathbf{R}^∞ is unimodal. Note that the i th column of \mathbf{R}^∞ can be written as $v_i \mathbf{v}$, where v_i is the i th entry of \mathbf{v} . We therefore confirm that \mathbf{v} is unimodal, with its n th entry being the peak.

Similarly, by constructing $\mathbf{Q} = \mathbf{H}\mathbf{H}^T$, we can also show that \mathbf{u} is unimodal with its m th entry being the peak. ■

APPENDIX B PROOF OF PROPOSITION 1

Consider uniformly shifting the discretization grid points $\{\mathbf{c}_{i,j}\}$ to such a position that the source location \mathbf{s}_k is the center of a rectangle formed by the four nearest grid points. Specifically, the new grid points are given by $\tilde{\mathbf{c}}_{i,j} = \mathbf{c}_{i,j} + \boldsymbol{\delta}$, where $\boldsymbol{\delta} = \mathbf{s}_k - \mathbf{c}_{m,n} - (\frac{L}{2N}, \frac{L}{2N})$, $m = \sup\{i : c_{X,i} \leq s_{k,1}\}$, and $n = \sup\{j : c_{Y,j} \leq s_{k,2}\}$. One can verify that \mathbf{s}_k is at the center of the rectangle formed by the four nearest grid points $\tilde{\mathbf{c}}_{m,n}$, $\tilde{\mathbf{c}}_{m+1,n}$, $\tilde{\mathbf{c}}_{m,n+1}$, and $\tilde{\mathbf{c}}_{m+1,n+1}$.

A. The Symmetry Property

Let $\tilde{\mathbf{H}}^{(k)}$ be the virtual signature matrix defined on the shifted grid points $\{\tilde{\mathbf{c}}_{i,j}\}$ using (3). As illustrated in Fig. 5, consider a sub-block $\tilde{\mathbf{H}}_1^{(k)}$ that contains the $(m+1-J_1)$ th to $(m+J_1)$ th rows and the $(n+1-J_2)$ th to $(n+J_2)$ th columns of $\tilde{\mathbf{H}}^{(k)}$, where $J_1 = \min\{m, \frac{N}{2}\}$ and $J_2 = \min\{n, \frac{N}{2}\}$. Further divide the $2J_1 \times 2J_2$ sub-block $\tilde{\mathbf{H}}_1^{(k)}$ into four $J_1 \times J_2$ sub-blocks. Since the locations $\tilde{\mathbf{c}}_{i,j}$ that correspond to the entries of $\tilde{\mathbf{H}}_1^{(k)}$ are symmetric about the source \mathbf{s}_k , one can verify that $\tilde{\mathbf{H}}_1^{(k)}$ has the following structure

$$\tilde{\mathbf{H}}_1^{(k)} = \begin{bmatrix} \tilde{\mathbf{H}}_{11}^{(k)} & \Pi_c(\tilde{\mathbf{H}}_{11}^{(k)}) \\ \Pi_r(\tilde{\mathbf{H}}_{11}^{(k)}) & \Pi_r(\Pi_c(\tilde{\mathbf{H}}_{11}^{(k)})) \end{bmatrix} \quad (31)$$

where the operators $\Pi_c(\mathbf{A})$ reverses the columns of \mathbf{A} and $\Pi_r(\mathbf{A})$ reverses the rows of \mathbf{A} .

Lemma 4. Let $\tilde{\mathbf{H}}_{11}^{(k)} = \mathbf{U}\boldsymbol{\Sigma}\mathbf{V}^T$ be the SVD of $\tilde{\mathbf{H}}_{11}^{(k)}$. Then,

$$\tilde{\mathbf{H}}_1^{(k)} = \begin{bmatrix} \mathbf{U} \\ \Pi_r(\mathbf{U}) \end{bmatrix} \boldsymbol{\Sigma} \begin{bmatrix} \mathbf{V}^T & \Pi_r(\mathbf{V})^T \end{bmatrix} \quad (32)$$

where, on the right hand side, the left and the right matrices are semi-orthogonal, respectively.

Proof. First, one can verify that the left-bottom sub-block of $\tilde{\mathbf{H}}_1^{(k)}$ in (31) satisfies $\Pi_r(\tilde{\mathbf{H}}_{11}^{(k)}) = \Pi_r(\mathbf{U})\boldsymbol{\Sigma}\mathbf{V}^T$, since the (i,j) th entry is given by

$$\begin{aligned} [\Pi_r(\tilde{\mathbf{H}}_{11}^{(k)})]_{i,j} &= [\tilde{\mathbf{H}}_{11}^{(k)}]_{J_1+1-i,j} \\ &= \sum_{l=1}^{\min\{J_1, J_2\}} U_{J_1+1-i,l} \Sigma_{l,l} V_{j,l} \\ &= \sum_{l=1}^{\min\{J_1, J_2\}} [\Pi_r(\mathbf{U})]_{i,l} \Sigma_{l,l} V_{j,l} \\ &= [\Pi_r(\mathbf{U})\boldsymbol{\Sigma}\mathbf{V}^T]_{i,j}. \end{aligned}$$

Similarly, one can verify that other sub-blocks of $\tilde{\mathbf{H}}_1^{(k)}$ agree with the decomposition (32).

Second, to see the semi-orthogonality, one can compute

$$\begin{bmatrix} \mathbf{U} \\ \Pi_r(\mathbf{U}) \end{bmatrix}^T \begin{bmatrix} \mathbf{U} \\ \Pi_r(\mathbf{U}) \end{bmatrix} = \mathbf{U}^T \mathbf{U} + \Pi_r(\mathbf{U})^T \Pi_r(\mathbf{U}) \\ = 2\mathbf{U}^T \mathbf{U} = 2\mathbf{I}.$$

Similarly, one can verify the semi-orthogonality of $\begin{bmatrix} \mathbf{V}^T & \Pi_r(\mathbf{V})^T \end{bmatrix}^T$. □

As a result, the dominant singular vectors of $\tilde{\mathbf{H}}_1^{(k)}$ are $\tilde{\mathbf{u}}_k^1 = \frac{1}{\sqrt{2}}[\mathbf{u}_1^T, \Pi_r(\mathbf{u}_1)^T]^T$ and $\tilde{\mathbf{v}}_k^1 = \frac{1}{\sqrt{2}}[\mathbf{v}_1^T, \Pi_r(\mathbf{v}_1)^T]^T$, where \mathbf{u}_1 and \mathbf{v}_1 are the first columns of \mathbf{U} and \mathbf{V} , respectively. It is clear that $\tilde{\mathbf{u}}_k^1$ and $\tilde{\mathbf{v}}_k^1$ are symmetric, respectively.

B. The Zero-padding Property

Consider building an unbounded lattice by extending the rows and columns of $\{\tilde{\mathbf{c}}_{i,j} : i, j = 1, 2, \dots, N\}$ to infinity with equal spacing $\frac{L}{N}$ (i.e., i, j take all the integer values). We construct a $2J \times 2J$ matrix $\bar{\mathbf{H}}^{(k)}$, $J = N - \min\{m, n\}$, using the $2J \times 2J$ array of elements $\{\frac{L}{N} \alpha_k h(d(\tilde{\mathbf{c}}_{i,j}, \mathbf{s}_k)) : 1 - J \leq i - m, j - n \leq J\}$. Then, $\tilde{\mathbf{H}}_1^{(k)}$ is a sub-block of $\tilde{\mathbf{H}}^{(k)}$ which is a sub-block of $\bar{\mathbf{H}}^{(k)}$. Moreover, $\tilde{\mathbf{H}}_1^{(k)}$ is a sub-block at the center of $\bar{\mathbf{H}}^{(k)}$.

Lemma 5. Except sub-block $\tilde{\mathbf{H}}_1^{(k)}$, the entries of $\bar{\mathbf{H}}^{(k)}$ are zero.

Proof. By the choices of J_1 and J_2 , the sub-block $\tilde{\mathbf{H}}_1^{(k)}$ covers the whole area that observes non-zero energy from the source. To see this, for any location $\tilde{\mathbf{c}}_{i,j}$ outside sub-block $\tilde{\mathbf{H}}_1^{(k)}$, either $\tilde{\mathbf{c}}_{i,j}$ or $\tilde{\mathbf{c}}_{i,\tilde{j}}$, the grid point symmetric about the source location \mathbf{s}_k , is outside the target area \mathcal{A} . We thus have $h(d(\tilde{\mathbf{c}}_{i,j}, \mathbf{s}_k)) = h(d(\tilde{\mathbf{c}}_{i,\tilde{j}}, \mathbf{s}_k)) = 0$ due to the assumption that $\int_{\mathbb{R}^2 \setminus \mathcal{A}} h(d(\mathbf{z}, \mathbf{s}))^2 d\mathbf{z} = 0$. □

Thus, the singular vectors of $\overline{\mathbf{H}}^{(k)}$ can be obtained from the singular vectors of $\tilde{\mathbf{H}}_1^{(k)}$ by padding zeros with proper dimensions: $\tilde{\mathbf{u}}_k^\Pi = [\mathbf{0}^\top, (\tilde{\mathbf{u}}_k^1)^\top, \mathbf{0}^\top]^\top$ and $\tilde{\mathbf{v}}_k^\Pi = [\mathbf{0}^\top, (\tilde{\mathbf{v}}_k^1)^\top, \mathbf{0}^\top]^\top$.

In addition, $\overline{\mathbf{H}}^{(k)}$ is symmetric because the (\tilde{i}, \tilde{j}) th entry is sampled at location $\tilde{\mathbf{c}}_{m-J+\tilde{i}, n-J+\tilde{j}}$ which has the same distance to the source \mathbf{s}_k as location $\tilde{\mathbf{c}}_{m-J+\tilde{j}, n-J+\tilde{i}}$ does. As a result, the dominant left and right singular vectors are equal, $\tilde{\mathbf{u}}_k^\Pi = \tilde{\mathbf{v}}_k^\Pi$. Since $\tilde{\mathbf{H}}_1^{(k)}$ is a sub-block of $\tilde{\mathbf{H}}^{(k)}$ which is a sub-block of $\overline{\mathbf{H}}^{(k)}$, the dominant singular vectors of $\tilde{\mathbf{H}}^{(k)}$ equals to some portions of the common vector $\tilde{\mathbf{u}}_k^\Pi$, where the left singular vector $\tilde{\mathbf{u}}_k$ is symmetric about the n th element, and the right singular vector $\tilde{\mathbf{v}}_k$ the m th element.

C. Convergence Analysis

Finally, we study the perturbation or error $\tilde{\mathbf{H}}^{(k)} - \mathbf{H}^{(k)}$. Denote $\tilde{u}_k^N(y)$ and $\tilde{v}_k^N(x)$ as linearly interpolated functions from the singular vectors $\tilde{\mathbf{u}}_k$ and $\tilde{\mathbf{v}}_k$, respectively, *i.e.*, $\tilde{u}_k^N(c_{Y,i} + \delta_1) = \sqrt{N/L}\tilde{u}_{k,i}$ and $\tilde{v}_k^N(c_{X,j} + \delta_2) = \sqrt{N/L}\tilde{v}_{k,j}$. A perturbation analysis yields

$$\begin{aligned} |H_{ij}^{(k)} - \tilde{H}_{ij}^{(k)}| &= \frac{L}{N} \alpha_k \left| h(d_{ij}) \right. \\ &\quad \left. - \left(h(d_{ij}) + \int_0^1 h'(d_{ij} + t\tilde{\delta}_{ij}) dt \right) \right| \\ &\leq \frac{\alpha_k K_h L}{N} |\tilde{\delta}_{ij}| \\ &\leq \frac{\alpha_k K_h L^2}{\sqrt{2}N^2} \end{aligned} \quad (33)$$

where $d_{ij} = \|\mathbf{c}_{i,j} - \mathbf{s}_k\|$, $\tilde{\delta}_{ij} = \|\tilde{\mathbf{c}}_{i,j} - \mathbf{s}_k\| - d_{ij}$, and $h'(d) = \lim_{t \downarrow 0} \frac{1}{t} [h(d+t) - h(d)]$ denotes the right derivative of $h(d)$. The upper bound (33) implies that $\mathbf{H}^{(k)}$ converges to $\tilde{\mathbf{H}}^{(k)}$, in the sense that $\|\mathbf{H}^{(k)} - \tilde{\mathbf{H}}^{(k)}\|_F^2 \leq N^2 \left(\frac{\alpha_k K_h L^2}{\sqrt{2}N^2} \right)^2 = \frac{C_H}{N^2} \rightarrow 0$. In addition, since $\tilde{u}_k^N(y)$ and $\tilde{v}_k^N(x)$ uniformly converge, we must have $\tilde{u}_k^N(y) \rightarrow \tilde{u}_k^N(y)$ and $\tilde{v}_k^N(x) \rightarrow \tilde{v}_k^N(x)$, uniformly as $N \rightarrow \infty$.

Note that since $\tilde{\mathbf{u}}_k$ and $\tilde{\mathbf{v}}_k$ are extracted from the common vector $\tilde{\mathbf{u}}_k^\Pi$, the interpolated functions $\tilde{u}_k^N(y)$ $\tilde{v}_k^N(x)$ has an identical shape. Therefore, there exists a unimodal symmetric function $w(x) = w(-x)$, such that $\tilde{u}_k^N(y) \rightarrow w(y - s_{k,2})$ and $\tilde{v}_k^N(x) \rightarrow w(x - s_{k,1})$. The property $\int_{-\infty}^{\infty} w(x)^2 dx = 1$ is a direct consequence of the unit norm of singular vectors. ■

APPENDIX C PROOF OF THEOREM 2

We first compute the peak localization error bound given the signature vector perturbations.

Let $\hat{\mathbf{v}}_1$ be the dominant right singular vector of \mathbf{H} , the observation matrix in the case of conservative construction, where $N = \sqrt{M}$. In the case of aggressive construction, $N > \sqrt{M}$, let $\hat{\mathbf{v}}_1$ be the dominant right singular vector of $\hat{\mathbf{X}}$, the solution to $\mathcal{P}2$. Denote $\mathbf{e}_1 = \hat{\mathbf{v}}_1 - \mathbf{v}_1$.

From (12), it follows that

$$\begin{aligned} R(t; \hat{\mathbf{v}}_1) &= \int_{-\infty}^{\infty} \left(w_1(x) + \bar{e}_1^N(x) \right) \left(w_1(-x+t) + \bar{e}_1^N(-x+t) \right) dx \\ &= \int_{-\infty}^{\infty} w_1(x) w_1(-x+t) dx + \int_{-\infty}^{\infty} w_1(x) \bar{e}_1^N(-x+t) dx \\ &\quad + \int_{-\infty}^{\infty} \bar{e}_1^N(x) w_1(-x+t) dx + \int_{-\infty}^{\infty} \bar{e}_1^N(x) \bar{e}_1^N(-x+t) dx \\ &= \tau(t - 2s_{1,1}) + \int_{-\infty}^{\infty} w_1(x) \bar{e}_1^N(-x+t) dx \\ &\quad + \int_{+\infty}^{-\infty} \bar{e}_1^N(-y+t) w_1(y) (-dy) + E^N(t) \\ &= \tau(t - 2s_{1,1}) + 2 \int_{-\infty}^{\infty} w_1(x) \bar{e}_1^N(-x+t) dx + E^N(t) \end{aligned} \quad (34)$$

where Equation (35) uses the fact that $\int_{-\infty}^{\infty} w_1(x) w_1(-x+t) dx = \tau(t - 2s_{1,1})$ from the integral (9).

As $t = 2\hat{s}_{1,1}$ maximizes $R(t; \hat{\mathbf{v}}_1)$ in (35), we have

$$\begin{aligned} &\tau(2\hat{s}_{1,1} - 2s_{1,1}) \\ &+ 2 \int_{-\infty}^{\infty} w_1(x) \bar{e}_1^N(-x + 2\hat{s}_{1,1}) dx + E^N(2\hat{s}_{1,1}) - E^N(2s_{1,1}) \\ &\geq \tau(2s_{1,1} - 2s_{1,1}) + 2 \int_{-\infty}^{\infty} w_1(x) \bar{e}_1^N(-x + 2s_{1,1}) dx \\ &= \tau(0) + 2 \int_{-\infty}^{\infty} w_1(x) \bar{e}_1^N(-x + 2s_{1,1}) dx \end{aligned}$$

where $\tau(0) = \int_{-\infty}^{\infty} w_1(x)^2 dx = 1$. As a result,

$$\begin{aligned} &1 - \tau(2\hat{s}_{1,1} - 2s_{1,1}) \\ &\leq 2 \int_{-\infty}^{\infty} w_1(x) \left[e(-x + 2\hat{s}_{1,1}) - e(-x + 2s_{1,1}) \right] dx \\ &\quad + E^N(2s_{1,1}) - E^N(2\hat{s}_{1,1}) \\ &\leq 2C_e |(\mathbf{v}_1^N)^\top \mathbf{e}_1^N| + o(|(\mathbf{v}_1^N)^\top \mathbf{e}_1^N|) \end{aligned}$$

using conditions (17) and (18) for asymptotically large N . We obtain

$$1 - 2C_e |(\mathbf{v}_1^N)^\top \mathbf{e}_1^N| + o(|(\mathbf{v}_1^N)^\top \mathbf{e}_1^N|) \leq \tau(2|\hat{s}_{1,1} - s_{1,1}|) \quad (36)$$

which leads to $|\hat{s}_{1,1} - s_{1,1}| \leq \frac{1}{2} \tau^{-1}(1 - 2C_e |(\mathbf{v}_1^N)^\top \mathbf{e}_1^N| + o(|(\mathbf{v}_1^N)^\top \mathbf{e}_1^N|))$, where $t = \tau^{-1}(y)$ is the inverse function of $y = \tau(t)$, $t \geq 0$. Hence,

$$(\hat{s}_{1,1} - s_{1,1})^2 \leq \frac{1}{4} \left[\tau^{-1}(1 - 2C_e \phi_0 + o(\phi_0)) \right]^2 \quad (37)$$

where we denote $\phi_0 \triangleq |(\mathbf{v}_1^N)^\top \mathbf{e}_1^N|$.

In addition, from the assumption that the first and the second-order derivatives, $\tau'(t)$ and $\tau''(t)$, exist and are continuous at $t = 0$, we bound $\tau(t)$ by a quadratic function

$$\tau(t) \leq \tau(0) + \tau'(0)t + \frac{1}{2}(\tau''(0) + \nu)t^2 \quad (38)$$

for some small $\nu > 0$. Note that for any ν , there exists $a_\nu > 0$, such that the quadratic upper bound (38) holds for all $t \in$

$[0, a_\nu]$. In addition, from the definition of $\tau(t)$ in (8), we obtain $\tau(0)' = 0$ and $\tau''(0) < 0$. Then, from (36), we arrive at

$$\begin{aligned} 1 - 2C_e\phi_0 + o(\phi_0) &\leq \tau(2|\hat{s}_{1,1} - s_{1,1}|) \\ &\leq 1 + \frac{1}{2}(\tau''(0) + \nu) \times 4(\hat{s}_{1,1} - s_{1,1})^2 \end{aligned} \quad (39)$$

if $t = 2|\hat{s}_{1,1} - s_{1,1}|$ is small enough, i.e., $t \in [0, a_\nu]$. Note that $\tau''(0) + \nu < 0$ as ν can be chosen arbitrarily small. As a result,

$$|\hat{s}_{1,1} - s_{1,1}|^2 \leq \frac{1}{2} \frac{(2C_e\phi_0 + o(\phi_0))}{-\tau''(0) - \nu} = \frac{1}{2} \frac{(2C_e + o(1))\phi_0}{-\tau''(0) - \nu}.$$

For small enough ϕ_0 , we will have $|o(\phi_0)| < C_e$, which yields

$$|\hat{s}_{1,1} - s_{1,1}|^2 \leq \frac{1}{2} \cdot \frac{3C_e\phi_0}{-\tau''(0) - \nu}. \quad (40)$$

A similar result can be derived for the error component $(\hat{s}_{1,2} - s_{1,2})^2$ by analyzing the perturbation of \mathbf{u}_1 , and the result is statistically identical to (37) and (40). Combining (37) and (40) yields

$$\|\hat{\mathbf{s}}_1 - \mathbf{s}_1\|_2^2 \leq \max \left\{ \frac{3C_e\phi_0}{-\tau''(0) - \nu}, \frac{1}{2} \left[\tau^{-1}(1 - 2C_e\phi_0 + o(\phi_0)) \right]^2 \right\}. \quad (41)$$

Moreover, for small enough $\phi_0 = |(\mathbf{v}_1^N)^T \mathbf{e}_1^N|$, (41) simplifies to

$$\|\hat{\mathbf{s}}_1 - \mathbf{s}_1\|_2^2 \leq \frac{3C_e\phi_0}{-\tau''(0) - \nu}. \quad (42)$$

We hereafter drop the superscript N from \mathbf{v}_1^N and \mathbf{e}_1^N for simplicity and derive the signature perturbation $\phi_0 = |\mathbf{v}_1^T \mathbf{e}_1|$ by examining two cases.

A. The Case of Conservative Construction $N = \sqrt{M}$

Consider that the sensing location $\mathbf{z}^{(m)}$ is inside the grid cell centered at $\mathbf{c}_{i,j}$. Then, according to the matrix observation model (1)–(3), we have

$$\begin{aligned} H_{ij} - H_{ij} &= \frac{L}{N} \left(h^{(m)} - \alpha_1 h(d_{ij}) \right) \\ &= \frac{\alpha_1 L}{N} \left(\int_0^1 h'(d_{ij} + t\delta^{(m)}) dt + \frac{\mathbf{n}^{(m)}}{\alpha_1} \right) \\ &= \frac{\alpha_1 L}{N} \left(\Xi_{ij} + \frac{\mathbf{n}^{(m)}}{\alpha_1} \right) \end{aligned} \quad (43)$$

where $d_{ij} = \|\mathbf{c}_{i,j} - \mathbf{s}_1\|_2$, $\delta^{(m)} = \|\mathbf{z}^{(m)} - \mathbf{s}_1\|_2 - d_{ij}$, $h'(d) = \lim_{t \downarrow 0} \frac{1}{t} [h(t+d) - h(d)]$ is the right derivative of $h(d)$, and $\Xi_{ij} \triangleq \int_0^1 h'(d_{ij} + t\delta^{(m)}) dt$.

Note that by the Lipschitz continuity of $h(d)$, we have

$$|\Xi_{ij}| \leq K_h \delta^{(m)} \leq K_h L / (\sqrt{2}N) \quad (44)$$

and therefore, Ξ_{ij} is a *sub-Gaussian* random variable with sub-Gaussian moment bounded by $K_h L / (\sqrt{2}N)$ [27], [28].⁴

⁴Recall that a real-valued random variable X is said to be sub-Gaussian if it has the property that there is some $b > 0$ such that for every $t \in \mathbb{R}$ one has $\mathbb{E}\{e^{tX}\} \leq \exp(\frac{1}{2}b^2 t^2)$. The sub-Gaussian moment of X is defined as $s_G(X) = \inf\{b \geq 0 \mid \mathbb{E}\{e^{tX}\} \leq \exp(\frac{1}{2}b^2 t^2), \forall t \in \mathbb{R}\}$, which has property $s_G(aX) = |a|s_G(X)$ [27], [28].

In addition, the bounded random variable $\mathbf{n}^{(m)}$ is also sub-Gaussian with sub-Gaussian moment bounded by $\bar{\sigma}_n$. As a result, the random quantity $\frac{\alpha_1 L}{N} \Xi_{ij} + \frac{\alpha_1 L}{N} \frac{\mathbf{n}^{(m)}}{\alpha_1}$ from (43) is sub-Gaussian with sub-Gaussian moment bounded by⁵

$$\bar{\omega} \triangleq \frac{\alpha_1 L}{N} \sqrt{\left(\frac{K_h L}{\sqrt{2}N}\right)^2 + \left(\frac{\bar{\sigma}_n}{\alpha_1}\right)^2}. \quad (45)$$

Consider the $N \times N$ matrix of the sample error $\mathbf{E} \triangleq \mathbf{H} - \mathbf{H}$, where the entries E_{ij} have zero mean and sub-Gaussian moment bounded by $\bar{\omega}$ in (45). This implies that $\tilde{\mathbf{E}} = \frac{1}{\bar{\omega}} \mathbf{E}$ have zero mean entries with sub-Gaussian moment bounded by 1. A bound of the spectral norm $\sigma(\tilde{\mathbf{E}})$ can be derived using the following result.

Lemma 6 (Spectral Norm [29]). *For an $N \times n$ random matrix \mathbf{X} whose entries are independent zero mean sub-Gaussian random variables with sub-Gaussian moments bounded by 1, it holds that*

$$\mathbb{P}\{\sigma(\mathbf{X}) > C(\sqrt{N} + \sqrt{n}) + t\} \leq 2e^{-ct^2}, \quad t \geq 0$$

for some universal constants C and c .

By choosing $N = n$ and $t = C\sqrt{N}$ in Lemma 6, we obtain $\sigma(\tilde{\mathbf{E}}) \leq 3C\sqrt{N}$ with probability at least $1 - 2e^{-cC^2N}$. Therefore,

$$\sigma(\mathbf{E})^2 \leq 9C^2 \bar{\omega}^2 N = C_0 \frac{\alpha_1^2 L^2}{N} \left(\frac{K_h^2 L^2}{2N^2} + \frac{\bar{\sigma}_n^2}{\alpha_1^2} \right) \quad (46)$$

holds with probability at least $1 - 2e^{-C_3N}$, where $C_0 = 9C^2$, and $C_3 = cC^2$.

We now derive an upper bound of $|\mathbf{v}_1^T \mathbf{e}_1|$.

Note that $\mathbf{v}_1^T \mathbf{e}_1 < 0$ because $1 = \|\hat{\mathbf{v}}_1\|_2^2 = \|\mathbf{v}_1 + \mathbf{e}_1\|_2^2 = 1 + 2\mathbf{v}_1^T \mathbf{e}_1 + \|\mathbf{e}_1\|_2^2$, and hence, $2\mathbf{v}_1^T \mathbf{e}_1 = -\|\mathbf{e}_1\|_2^2 < 0$. Then, the singular vector perturbation can be obtained as

$$\begin{aligned} \sin \angle(\mathbf{v}_1, \hat{\mathbf{v}}_1) &= \sqrt{1 - |\mathbf{v}_1^T(\mathbf{v}_1 + \mathbf{e}_1)|^2} \\ &= \sqrt{-2\mathbf{v}_1^T \mathbf{e}_1 + (\mathbf{v}_1^T \mathbf{e}_1)^2} \\ &\geq \sqrt{2|\mathbf{v}_1^T \mathbf{e}_1|} \end{aligned} \quad (47)$$

where $|\cdot|$ denotes the absolute value operator.

On the other hand, using the singular vector perturbation results in [30], we know that

$$\sin \angle(\mathbf{v}_1, \hat{\mathbf{v}}_1) \leq \frac{2\sigma(\mathbf{E})}{\sigma_{1,1} - \sigma_{1,2}} \quad (48)$$

where σ_1 and σ_2 are the first and second dominant singular values of \mathbf{H} . Recall that we have $\sigma_{1,1} - \sigma_{1,2} \rightarrow \kappa\alpha_1$, as $N \rightarrow \infty$.

Therefore, we arrive at

$$\begin{aligned} |\mathbf{v}_1^T \mathbf{e}_1| &\leq \frac{1}{2} \left(\sin \angle(\mathbf{v}_1, \hat{\mathbf{v}}_1) \right)^2 \\ &\leq \frac{1}{2} \left(\frac{2\sigma(\mathbf{E})}{\kappa\alpha_1} \right)^2 \\ &\leq \frac{C_0 K_h^2 L^4}{\kappa^2 N^3} + \frac{2C_0 L^2 \bar{\sigma}_n^2}{\kappa^2 N \alpha_1^2} \end{aligned}$$

⁵If X and Y are independent sub-Gaussian, the sub-Gaussian moment of $X + Y$ satisfies $s_G(X + Y) = \sqrt{s_G(X) + s_G(Y)}$ [27], [28].

for asymptotically large N , with probability at least $1 - 2e^{-C_3N}$. As $M = N^2$, it further holds that

$$3C_e |\mathbf{v}_1^T \mathbf{e}_1| \leq \frac{3C_0 C_e K_h^2 L^4}{\kappa^2 M^{1.5}} + \frac{6C_0 C_e L^2 \bar{\sigma}_n^2}{\kappa^2 \sqrt{M} \alpha_1^2} \triangleq \phi_1 \quad (49)$$

for large M with probability at least $1 - 2e^{-C_3N}$.

Note that for large enough M , the term ϕ_1 in (49) becomes small enough to satisfy $t = \tau^{-1}(1 - \phi_1) \leq a_\nu$, such that $\tau(t) \leq \tau(0) + \tau'(0)t + \frac{1}{2}(\tau''(0) + \nu)t^2$ holds, and therefore, (41) simplifies to (42). Applying $3C_e \phi_0 \leq \phi_1$ to (42) and using (49), we obtain (19).

B. The Case of Aggressive Construction $N > \sqrt{M}$

We first compute the total measurement noise using property (44) and the bounded noise assumption in Theorem 3. From (43), we have

$$\begin{aligned} (H_{ij} - H_{ij})^2 &= \frac{\alpha_1^2 L^2}{N^2} \left(\bar{\Xi}^2 + 2\Xi \frac{\mathbf{n}^{(m)}}{\alpha_1} + \left(\frac{\mathbf{n}^{(m)}}{\alpha_1} \right)^2 \right) \\ &\leq \frac{\alpha_1^2 L^2}{N^2} \left(\frac{K_h^2 L^2}{2N^2} + \frac{\sqrt{2} K_h L \bar{\sigma}_n}{N \alpha_1} + \frac{\bar{\sigma}_n^2}{\alpha_1^2} \right) \triangleq \bar{\epsilon}^2. \end{aligned} \quad (50)$$

As a result,

$$\|\mathcal{P}_\Omega(\mathbf{H} - \mathbf{H})\|_F^2 = \sum_{(i,j) \in \Omega} |H_{ij} - H_{ij}|^2 \leq M \bar{\epsilon}^2.$$

We then characterize the completed matrix $\hat{\mathbf{X}}$ as the solution to $\mathcal{P}2$.

Lemma 7 (Matrix completion with noise [21]). *Suppose that the parameter ϵ in $\mathcal{P}2$ is chosen to satisfy $\epsilon \geq \|\mathcal{P}_\Omega(\mathbf{H} - \mathbf{H})\|_F$. In addition, assume that $M \geq CN(\log N)^2$ for some constant $C = C'\beta$. Then, with probability at least $1 - N^{-\beta}$,*

$$\|\hat{\mathbf{X}} - \mathbf{H}\|_F \leq 4\sqrt{\frac{(2+p)N}{p}}\epsilon + 2\epsilon \quad (51)$$

where $p = M/N^2$.

According to Lemma 7, we choose the parameter $\epsilon = \sqrt{M}\bar{\epsilon}$ in $\mathcal{P}2$ for (51) to hold. In addition, the bound in (51) can be simplified as

$$\begin{aligned} \|\hat{\mathbf{X}} - \mathbf{H}\|_F &\leq 4\sqrt{\frac{(2+p)N}{p}}\epsilon + 2\epsilon \\ &= \left(4\sqrt{\frac{2N^3}{M} + N + 2} \right) \epsilon \end{aligned} \quad (52)$$

$$\leq \left(4\sqrt{\frac{2N^3}{CN(\log N)^2} + N + 2} \right) \epsilon \quad (53)$$

$$\begin{aligned} &= \left(\sqrt{\frac{32}{C} \frac{N}{\log N}} + o(\sqrt{N}) \right) \sqrt{M}\bar{\epsilon} \\ &\triangleq \bar{\eta} \end{aligned} \quad (54)$$

where equality (52) is based on the relation $p = M/N^2$, inequality (53) is due to $M \geq CN(\log N)^2$, and equality (54) can be shown using the following lemma.

Lemma 8. *Suppose that non-negative functions f and g satisfy $f(x) \rightarrow \infty$, $g(x) \rightarrow \infty$, and $h(x) = f(x)/g(x) \rightarrow \infty$, as $x \rightarrow \infty$. Then, $\sqrt{f(x) + g(x)} = \sqrt{f(x)} + o(\sqrt{g(x)})$, where $\lim_{x \rightarrow \infty} o(\sqrt{g(x)})/\sqrt{g(x)} = 0$.*

Proof. We can show that the residual error $\sqrt{f(x) + g(x)} - \sqrt{f(x)}$ grows slower than $\sqrt{g(x)}$ as follows

$$\begin{aligned} &\lim_{x \rightarrow \infty} \frac{\sqrt{f(x) + g(x)} - \sqrt{f(x)}}{\sqrt{g(x)}} \\ &= \lim_{x \rightarrow \infty} \sqrt{\frac{f(x)}{g(x)} + 1} - \sqrt{\frac{f(x)}{g(x)}} \\ &= \lim_{x \rightarrow \infty} \frac{(\sqrt{h(x) + 1} - \sqrt{h(x)})(\sqrt{h(x) + 1} + \sqrt{h(x)})}{\sqrt{h(x) + 1} + \sqrt{h(x)}} \\ &= \lim_{x \rightarrow \infty} \frac{1}{\sqrt{h(x) + 1} + \sqrt{h(x)}} \\ &= 0. \end{aligned} \quad \square$$

Let

$$f(N) = \frac{2N^3}{CN(\log N)^2} = \frac{2N^2}{C(\log N)^2}$$

and $g(N) = N$. We have $f, g \rightarrow \infty$ and $f/g \rightarrow \infty$ for $N \rightarrow \infty$. Then, equality (54) follows from Lemma 8.

Consider $\hat{\mathbf{E}}$ as a random matrix whose entries are independent zero mean with sub-Gaussian moments bounded by $\tilde{\omega} \triangleq \bar{\eta}/N$. Since $\frac{1}{N^2} \sum_{i,j} |\hat{X}_{ij} - H_{ij}|^2 \leq \bar{\eta}^2/N^2$ with probability at least $1 - N^{-\beta}$, we know $\sigma(\hat{\mathbf{X}} - \mathbf{H}) \leq \sigma(\hat{\mathbf{E}})$ with probability at least $1 - N^{-\beta}$. Following the same derivation as for (46), we obtain

$$\begin{aligned} \sigma(\hat{\mathbf{E}})^2 &\leq C_0 \tilde{\omega}^2 N = \frac{C_0}{N} \left(\frac{32N^2}{C(\log N)^2} + o(N) \right) CN(\log N)^2 \bar{\epsilon}^2 \\ &= \bar{\epsilon}^2 \left(32C_0 N^2 + o(N(\log N)^2) \right) \end{aligned}$$

with probability at least $(1 - 2e^{-C_3N})(1 - N^{-\beta})$, i.e., $1 - \mathcal{O}(N^{-\beta})$.

Using the singular vector under perturbation results in [30] and the expression for $\bar{\epsilon}$ in (50), and following similar calculations in (47)–(49), we obtain

$$\begin{aligned} |\mathbf{v}_1^T \mathbf{e}_1| &\leq \frac{1}{2} \left(\frac{2\sigma(\hat{\mathbf{E}})}{\kappa \alpha_1} \right)^2 \\ &= \frac{2L^2}{\kappa^2} \left(\frac{K_h^2 L^2}{2N^2} + \frac{\sqrt{2} K_h L \bar{\sigma}_n}{N \alpha_1} + \frac{\bar{\sigma}_n^2}{\alpha_1^2} \right) \\ &\quad \times \left(32C_0 + o\left(\frac{(\log N)^2}{N}\right) \right) \end{aligned} \quad (55)$$

with probability $1 - \mathcal{O}(N^{-\beta})$.

Finally, if one choose parameters M, N such that M is the smallest integer satisfying $M \geq CN(\log N)^2$, then we can write $M = CN(\log N)^2 + \epsilon_0$, where $\epsilon_0 \in [0, 1)$. As a result, from $M^{1-\alpha} = [CN(\log N)^2 + \epsilon_0]^{1-\alpha}$, we arrive at

$$\frac{M^{1-\alpha}}{N} = C^{1-\alpha} \frac{(\log N)^{2(1-\alpha)}}{N^\alpha} \left[1 + \frac{\epsilon_0}{CN(\log N)^2} \right]^{1-\alpha}. \quad (56)$$

It is clear that for $0 < \alpha < \frac{1}{2}$, the term $\frac{(\log N)^{2(1-\alpha)}}{N^\alpha}$ converges to 0 as $N \rightarrow \infty$. As a result, there exists a finite integer $N_1 < \infty$ such that for any $N > N_1$, the right hand side of (56) is less than 1, i.e., $\frac{M^{1-\alpha}}{N} \leq 1$. This implies that $\frac{1}{N} \leq \frac{1}{M^{1-\alpha}}$. Similarly, using $M^{2-\alpha} = [CN(\log N)^2 + \epsilon_0]^{2-\alpha}$, one can obtain $\frac{1}{N^2} \leq \frac{1}{M^{2-\alpha}}$ for asymptotically large M, N . Substituting $\frac{1}{N} \leq \frac{1}{M^{1-\alpha}}$ and $\frac{1}{N^2} \leq \frac{1}{M^{2-\alpha}}$ to (55) and omitting the $o(\cdot)$ term, one can obtain

$$3C_e |\mathbf{v}_1^T \mathbf{e}_1| \leq \frac{C'_0 C_e L^2}{\kappa^2} \left(\frac{K_h^2 L^2}{2M^{2-\alpha}} + \frac{\sqrt{2} K_h L \bar{\sigma}_n}{M^{1-\alpha} \alpha_1} + \frac{\bar{\sigma}_n^2}{\alpha_1^2} \right) \triangleq \phi_2 \quad (57)$$

with probability $1 - \mathcal{O}(N^{-\beta})$, where $C'_0 = 192C_0$.

Note that for large enough M and high SNR $\alpha_1/\bar{\sigma}_n$, the term ϕ_2 in (57) becomes small enough to satisfy $t = \tau^{-1}(1 - \phi_2) \leq a_\nu$, such that $\tau(t) \leq \tau(0) + \tau'(0)t + \frac{1}{2}(\tau''(0) + \nu)t^2$ holds, and therefore, (41) simplifies to (42). Applying $3C_e \phi_0 \leq \phi_2$ to (42) and using (57), we obtain (20).

APPENDIX D PROOF OF THEOREM 4

W.l.o.g., assume that the two sources are located at $\mathbf{s}_1 = (0, 0)$ and $\mathbf{s}_2 = (D \cos \theta, D \sin \theta)$. Define $w_c(x, \theta) = w(x - D \cos \theta)$ and $w_s(x, \theta) = w(x - D \sin \theta)$, where $w(x)$ is the unimodal and symmetric function defined in Proposition 1.

Using Proposition 1, we have the following approximation under large N

$$\begin{aligned} \|\mathbf{u}_1 + \mathbf{u}_2\|_2^2 &\approx \int_{-\infty}^{\infty} (w(x) + w_c(x, \theta))^2 dx \\ &\triangleq \langle (w + w_c)^2 \rangle \end{aligned}$$

where we have defined an integration operator $\langle \cdot \rangle$ as

$$\langle f \rangle \triangleq \int_{-\infty}^{\infty} f(x, \theta) dx$$

for a function $f(x, \theta)$. Note that the operator $\langle \cdot \rangle$ is linear and satisfies the additive property, i.e., $\langle af \rangle = a \langle f \rangle$ and $\langle f + g \rangle = \langle f \rangle + \langle g \rangle$, for a constant a and a function $g(x, \theta)$.

Similarly, $\|\mathbf{v}_1 + \mathbf{v}_2\|_2^2 \approx \langle (w + w_s)^2 \rangle$, $\|\mathbf{u}_1 - \mathbf{u}_2\|_2^2 \approx \langle (w - w_c)^2 \rangle$, and $\|\mathbf{v}_1 - \mathbf{v}_2\|_2^2 \approx \langle (w - w_s)^2 \rangle$.

In the case of $\alpha_1 = \alpha_2$, it can be shown that the SVD of \mathbf{H} is given by

$$\mathbf{H} = \sigma_1 \mathbf{p}_1 \mathbf{q}_1^T + \sigma_2 \mathbf{p}_2 \mathbf{q}_2^T \quad (58)$$

where $\sigma_1(\theta) = \frac{1}{2} \alpha_1 \|\mathbf{u}_1 + \mathbf{u}_2\|_2 \|\mathbf{v}_1 + \mathbf{v}_2\|_2$ and $\sigma_2(\theta) = \frac{1}{2} \alpha_1 \|\mathbf{u}_1 - \mathbf{u}_2\|_2 \|\mathbf{v}_1 - \mathbf{v}_2\|_2$ are the singular values, and

$$\mathbf{p}_1 = \frac{\mathbf{u}_1 + \mathbf{u}_2}{\|\mathbf{u}_1 + \mathbf{u}_2\|_2}, \quad \mathbf{q}_1 = \frac{\mathbf{v}_1 + \mathbf{v}_2}{\|\mathbf{v}_1 + \mathbf{v}_2\|_2}$$

$$\mathbf{p}_2 = \frac{\mathbf{u}_1 - \mathbf{u}_2}{\|\mathbf{u}_1 - \mathbf{u}_2\|_2}, \quad \mathbf{q}_2 = \frac{\mathbf{v}_1 - \mathbf{v}_2}{\|\mathbf{v}_1 - \mathbf{v}_2\|_2}$$

are the corresponding singular vectors. Here, all the components are functions of θ .

As a result,

$$\begin{aligned} \mu(\theta) &\triangleq \frac{\sigma_2(\theta)^2}{\sigma_1(\theta)^2} \\ &\approx \frac{\langle (w - w_c)^2 \rangle \langle (w - w_s)^2 \rangle}{\langle (w + w_c)^2 \rangle \langle (w + w_s)^2 \rangle} \\ &= \frac{(1 - \langle w \cdot w_c \rangle)(1 - \langle w \cdot w_s \rangle)}{(1 + \langle w \cdot w_c \rangle)(1 + \langle w \cdot w_s \rangle)} \end{aligned} \quad (59)$$

where we have used the fact that $\langle (w - w_c)^2 \rangle = \langle w^2 \rangle + \langle w_c^2 \rangle - 2 \langle w \cdot w_c \rangle = 2(1 - \langle w \cdot w_c \rangle)$.

In addition, from properties of calculus, if $f(x, \theta)$ and $\frac{\partial}{\partial \theta} f(x, \theta)$ are continuous in θ , then

$$\begin{aligned} \frac{d}{d\theta} \langle f \rangle &= \frac{d}{d\theta} \int_{-\infty}^{\infty} f(x, \theta) dx \\ &= \int_{-\infty}^{\infty} \frac{\partial}{\partial \theta} f(x, \theta) dx = \left\langle \frac{\partial}{\partial \theta} f \right\rangle. \end{aligned}$$

Therefore, defining

$$\begin{aligned} w'_c(x, \theta) &\triangleq \frac{d}{dx} w(x) \Big|_{x=x-D \cos \theta} \\ w'_s(x, \theta) &\triangleq \frac{d}{dx} w(x) \Big|_{x=x-D \sin \theta} \end{aligned}$$

we have

$$\begin{aligned} \frac{d}{d\theta} \langle w \cdot w_c \rangle &= \langle w \cdot \frac{\partial}{\partial \theta} w_c(x, \theta) \rangle = \langle w \cdot w'_c \rangle D \sin \theta \\ \frac{d}{d\theta} \langle w \cdot w_s \rangle &= \langle w \cdot \frac{\partial}{\partial \theta} w_s(x, \theta) \rangle = -\langle w \cdot w'_s \rangle D \cos \theta. \end{aligned}$$

With some algebra, the derivative of $\mu(\theta)$ can be obtained as

$$\begin{aligned} \frac{d}{d\theta} \mu(\theta) &= \eta \left[D \cos \theta \langle w \cdot w'_s \rangle (1 - \langle w \cdot w_c \rangle)^2 \right. \\ &\quad \left. - D \sin \theta \langle w \cdot w'_c \rangle (1 - \langle w \cdot w_s \rangle)^2 \right] \\ &= \eta \left[-t \cdot \tau'(s) (1 - \tau(t)^2) + s \cdot \tau'(t) (1 - \tau(s)^2) \right] \end{aligned}$$

where $\eta = 2(1 + \langle w \cdot w_c \rangle)^{-2} (1 + \langle w \cdot w_s \rangle)^{-2}$, $t = D \cos \theta$, and $s = D \sin \theta$.

Note that $0 < s < t$ for $0 < \theta < \frac{\pi}{4}$. Applying condition (22), we have

$$\begin{aligned} \frac{d}{d\theta} \mu(\theta) &> \eta \cdot t \cdot \tau'(s) \left[(1 - \tau(s)^2) - (1 - \tau(t)^2) \right] \\ &= \eta \cdot t \cdot \tau'(s) (\tau(t)^2 - \tau(s)^2) \\ &> 0 \end{aligned}$$

since $\tau'(s) < 0$ and $\tau(t) < \tau(s)$ for $0 < s < t$.

This confirms that $\mu(\theta)$ is a strictly increasing function, and hence $\rho(\theta)$ is a strictly decreasing function in $\theta \in (0, \frac{\pi}{4})$. The result is thus proved. \blacksquare

APPENDIX E PROOF OF PROPOSITION 2

For notation brevity, we drop the symbol t for the variables related to the continuous-time algorithm dynamic $\mathbf{X}(t)$ wherever the meaning is clear.

Denote the Hessian function of $f(\mathbf{X})$ along the direction $\xi \in \mathbb{R}^{N \times N}$ as

$$h(\xi, \mathbf{X}) = \lim_{\gamma \rightarrow 0} \frac{1}{\gamma} \left[g(\mathbf{X} + \gamma \xi) - g(\mathbf{X}) \right].$$

Then, a Taylor's expansion of the gradient function $g(\mathbf{X})$ yields

$$g(\mathbf{X}) = g(\hat{\mathbf{X}}) + h(s\xi, \hat{\mathbf{X}}) + o(s)$$

where $\xi = \frac{1}{\gamma}(\mathbf{X} - \hat{\mathbf{X}})$ and $\gamma = \|\mathbf{X} - \hat{\mathbf{X}}\|_F$. Therefore, as $g(\hat{\mathbf{X}}) = \mathbf{0}$, it holds that $g(\mathbf{X}) \approx h(\mathbf{X}_e, \hat{\mathbf{X}})$ for small s .

In addition, it holds that

$$\begin{aligned} \frac{d}{dt} \mathcal{E}(\mathbf{X}_e(t)) &= \text{tr} \left\{ (\mathbf{X}(t) - \hat{\mathbf{X}})^T \frac{d}{dt} \mathbf{X}(t) \right\} \\ &= -\text{tr} \left\{ (\mathbf{X}(t) - \hat{\mathbf{X}})^T g(\mathbf{X}(t)) \right\}. \end{aligned}$$

As a result, $\frac{d}{dt} \mathcal{E}(\mathbf{X}_e) = -\text{tr} \left\{ \mathbf{X}_e^T h(\mathbf{X}_e^T, \hat{\mathbf{X}}) \right\} + o(\|\mathbf{X}_e\|_F^2)$.

Using (25) – (26) and the fact that $\mathbf{H} = \hat{\mathbf{U}} \hat{\mathbf{V}}^T$, it can be shown that

$$\begin{aligned} \frac{1}{2} \text{tr} \left\{ \mathbf{X}_e^T h(\mathbf{X}_e, \mathbf{X}) \right\} &= \text{tr} \left\{ \mathbf{U}_e^T (\mathbf{W} \odot (\mathbf{U}_e \mathbf{V}^T)) \mathbf{V} \right. \\ &\quad \left. + \mathbf{V}_e^T (\mathbf{W}^T \odot (\mathbf{V}_e \mathbf{U}^T)) \mathbf{U} \right\} \\ &\quad + \text{tr} \left\{ \mathbf{U}_e^T (\mathbf{W} \odot (\mathbf{U} \mathbf{V}_e^T)) \mathbf{V} \right\} \\ &\quad + \text{tr} \left\{ \mathbf{V}_e^T (\mathbf{W}^T \odot (\mathbf{V} \mathbf{U}_e^T)) \mathbf{U} \right\}. \end{aligned}$$

Note that under $\mathbf{H} = \mathbf{H}$, we have $\mathbf{W} = \mathbf{1}_{N \times N}$. In addition, if $\|\mathbf{V}_e\|_F = o(\|\mathbf{U}_e\|_F)$, i.e., $\|\mathbf{V}_e\|_F \ll \|\mathbf{U}_e\|_F$, then

$$\begin{aligned} \frac{1}{2} \text{tr} \left\{ \mathbf{X}_e^T h(\mathbf{X}_e, \mathbf{X}) \right\} &= \text{tr} \left\{ \mathbf{U}_e^T \mathbf{U}_e \mathbf{V}^T \mathbf{V} \right\} + o(\|\mathbf{U}_e\|_F^2) \\ &= \text{tr} \left\{ \mathbf{U}_e \mathbf{V}^T \mathbf{V} \mathbf{U}_e \right\} + o(\|\mathbf{U}_e\|_F^2) \\ &= \sum_{j=1}^N \mathbf{u}_j^{(e)} \mathbf{V}^T \mathbf{V} \mathbf{u}_j^{(e)T} + o(\|\mathbf{U}_e\|_F^2) \\ &\geq \sum_{j=1}^N \lambda_K(\mathbf{V}^T \mathbf{V}) \|\mathbf{u}_j^{(e)}\|^2 + o(\|\mathbf{U}_e\|_F^2) \end{aligned}$$

where $\mathbf{u}_j^{(e)}$ is the j th row vector of the matrix \mathbf{U}_e . As a result, we have

$$\frac{d}{dt} \mathcal{E}(\mathbf{X}_e) \leq -2\lambda_K(\hat{\mathbf{V}} \hat{\mathbf{V}}^T) \|\mathbf{U}_e\|_F^2 + o(\|\mathbf{U}_e\|_F^2)$$

proving (28).

For the case of $\|\mathbf{U}_e\|_F = o(\|\mathbf{V}_e\|_F)$, the derivation to show (29) is similar. ■

REFERENCES

- [1] A. Beck, P. Stoica, and J. Li, "Exact and approximate solutions of source localization problems," *IEEE Trans. Signal Process.*, vol. 56, no. 5, pp. 1770–1778, 2008.
- [2] X. Sheng and Y.-H. Hu, "Maximum likelihood multiple-source localization using acoustic energy measurements with wireless sensor networks," *IEEE Trans. Signal Process.*, vol. 53, no. 1, pp. 44–53, 2005.
- [3] C. Meesookho, U. Mitra, and S. Narayanan, "On energy-based acoustic source localization for sensor networks," *IEEE Trans. Signal Process.*, vol. 56, no. 1, pp. 365–377, 2008.
- [4] C. Liu, Y. V. Zakharov, and T. Chen, "Broadband underwater localization of multiple sources using basis pursuit de-noising," *IEEE Trans. Signal Process.*, vol. 60, no. 4, pp. 1708–1717, 2012.
- [5] H. Chen, Q. Shi, R. Tan, H. V. Poor, and K. Sezaki, "Mobile element assisted cooperative localization for wireless sensor networks with obstacles," *IEEE Trans. Wireless Commun.*, vol. 9, no. 3, 2010.
- [6] T. He, C. Huang, B. M. Blum, J. A. Stankovic, and T. Abdelzaher, "Range-free localization schemes for large scale sensor networks," in *Proc. Int. Conf. Mobile Computing and Networking*, 2003, pp. 81–95.
- [7] J. Wang, P. Urriza, Y. Han, and D. Cabric, "Weighted centroid localization algorithm: theoretical analysis and distributed implementation," *IEEE Trans. Wireless Commun.*, vol. 10, no. 10, pp. 3403–3413, 2011.
- [8] S. Choudhary and U. Mitra, "Analysis of target detection via matrix completion," in *Proc. IEEE Int. Conf. Acoustics, Speech, and Signal Processing*, 2015, pp. 3771–3775.
- [9] J. Chen and U. Mitra, "Rotated eigenstructure analysis for source localization without energy-decay models," in *Proc. Int. Conf. Digital Signal Process.*, London, UK, Aug. 2017.
- [10] Y. Jin, W.-S. Soh, and W.-C. Wong, "Indoor localization with channel impulse response based fingerprint and nonparametric regression," *IEEE Trans. Wireless Commun.*, vol. 9, no. 3, pp. 1120–1127, 2010.
- [11] W. Kim, J. Park, J. Yoo, H. J. Kim, and C. G. Park, "Target localization using ensemble support vector regression in wireless sensor networks," *IEEE Trans. on Cybernetics*, vol. 43, no. 4, pp. 1189–1198, 2013.
- [12] S. H. Abadi, D. Rouseff, and D. R. Dowling, "Blind deconvolution for robust signal estimation and approximate source localization," *J. of Acoustical Society of America*, vol. 131, no. 4, pp. 2599–2610, 2012.
- [13] A. Ahmed, B. Recht, and J. Romberg, "Blind deconvolution using convex programming," *IEEE Trans. Inf. Theory*, vol. 60, no. 3, pp. 1711–1732, 2014.
- [14] Y. Li and Y. Chi, "Off-the-grid line spectrum denoising and estimation with multiple measurement vectors," *IEEE Trans. Signal Process.*, vol. 64, no. 5, pp. 1257–1269, 2016.
- [15] G. Tang, B. N. Bhaskar, P. Shah, and B. Recht, "Compressed sensing off the grid," *IEEE Trans. Inf. Theory*, vol. 59, no. 11, pp. 7465–7490, 2013.
- [16] D. Yang, G. Tang, and M. B. Wakin, "Super-resolution of complex exponentials from modulations with unknown waveforms," *IEEE Trans. Inf. Theory*, vol. 62, no. 10, pp. 5809–5830, 2016.
- [17] A. Cichocki, R. Zdunek, and S.-i. Amari, "New algorithms for non-negative matrix factorization in applications to blind source separation," in *Proc. IEEE Int. Conf. Acoustics, Speech, and Signal Processing*, vol. 5, 2006, pp. 621–624.
- [18] S. Choudhary, N. Kumar, S. Narayanan, and U. Mitra, "Active target localization using low-rank matrix completion and unimodal regression," *arXiv preprint arXiv:1601.07254*, 2016.
- [19] J. Chen and U. Mitra, "Underwater acoustic source localization using unimodal-constrained matrix factorization," in *Proc. Asilomar Conf. Signals, Systems and Computers*, Pacific Grove, CA, USA, Nov. 2017.
- [20] E. Candes and B. Recht, "Exact matrix completion via convex optimization," *Commun. of the ACM*, vol. 55, no. 6, pp. 111–119, 2012.
- [21] E. J. Candes and Y. Plan, "Matrix completion with noise," *Proceedings of the IEEE*, vol. 98, no. 6, pp. 925–936, 2010.
- [22] D. Bertsekas, *Nonlinear Programming*. Athena Scientific, 1999.
- [23] S. Boyd and L. Vandenberghe, *Convex Optimization*. Cambridge University Press, 2004.
- [24] A. Németh and S. Németh, "How to project onto an isotone projection cone," *Linear Algebra and its Applications*, vol. 433, no. 1, pp. 41–51, 2010.
- [25] S. Beygi and U. Mitra, "Multi-scale multi-lag channel estimation using low rank approximation for OFDM," *IEEE Trans. Signal Process.*, vol. 63, no. 18, pp. 4744–4755, 2015.
- [26] L. M. Brekhovskikh, *Fundamentals of ocean acoustics*. Springer Science & Business Media, 2003.
- [27] V. V. Buldygin and Y. V. Kozachenko, "Sub-Gaussian random variables," *Ukrainian Mathematical Journal*, vol. 32, no. 6, pp. 483–489, 1980.
- [28] K. Stromberg, *Probability for analysts*. CRC Press, 1994.
- [29] M. Rudelson and R. Vershynin, "Non-asymptotic theory of random matrices: extreme singular values," *Proceedings of the Int. Congress of Mathematicians, preprint arXiv:1003.2990*, pp. 1576–1602, 2010.
- [30] V. Vu, "Singular vectors under random perturbation," *Random Structures & Algorithms*, vol. 39, no. 4, pp. 526–538, 2011.